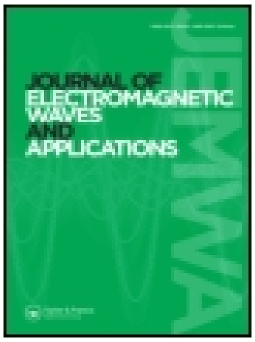


Journal of Electromagnetic Waves and Applications

ISSN: (Print) (Online) Journal homepage: https://www.tandfonline.com/loi/tewa20

Millimeter wave traveling wave tubes for the 21st Century

Claudio Paoloni , Diana Gamzina , Rosa Letizia , Yuan Zheng & Neville C. Luhmann Jr.

To cite this article: Claudio Paoloni , Diana Gamzina , Rosa Letizia , Yuan Zheng & Neville C. Luhmann Jr. (2020): Millimeter wave traveling wave tubes for the 21st Century, Journal of Electromagnetic Waves and Applications, DOI: 10.1080/09205071.2020.1848643

To link to this article: https://doi.org/10.1080/09205071.2020.1848643

Published online: 20 Dec 2020.

JOURNAL OF ELECTROMAGNETIC WAVES AND APPLICATIONS
https://doi.org/10.1080/09205071.2020.1848643

INVITED REVIEW ARTICLE

OPEN ACCESS

Millimeter wave traveling wave tubes for the 21st Century

Claudio Paoloni [a], Diana Gamzina[b], Rosa Letizia [a], Yuan Zheng [c] and Neville C. Luhmann Jr.[c]

[a]Engineering Department, Lancaster University, Lancaster, UK; [b]SLAC National Accelerator Laboratory, USA; [c]Department of Electrical Engineering, University of California, Davis, Davis, CA, USA

ABSTRACT

Traveling wave tubes are rapidly evolving to provide unprecedented power level in comparison to solid state devices in the millimeter waves region of the spectrum (80–300 GHz) thus enabling a wide range of applications.

Wireless communications, imaging, plasma diagnostics, healthcare and many others will gain substantial features if high power at millimeter waves would be available from compact sources.

The development of fabrication technologies is proving crucial for introducing new topologies and structures for millimeter wave vacuum electronic devices, compatible with the dimensions dictated by the short wavelength that poses substantial manufacturing challenges due to tight tolerances.

This review paper will provide an overview of the principles, evolution and state of the art of one of the most widely utilized vacuum electronic device, the traveling wave tube (TWT). The wide band, high gain features of TWTs make those devices the most promising solutions for high power at millimeter waves and THz frequencies.

ARTICLE HISTORY
Received 9 September 2020
Accepted 7 November 2020

KEYWORDS
Traveling wave tubes; millimeter waves; backward wave oscillators; vacuum electronics

1. Introduction

Microwave vacuum electron devices or microwave "tubes" utilize free electrons in a vacuum to convert energy from a dc power source to an RF signal. There exist a wide variety of microwave tubes including triodes, linear beam devices, crossed field devices, periodic beam devices, gyro devices, forward wave devices, and backward wave devices, as well as fast wave and slow wave devices. In the following, these terms will be briefly referred to the references for more details [1–5]. Most microwave vacuum tubes fit into more than one of these categories.

The energy conversion or "interaction" process differs markedly among microwave tubes. However, explanations of the various interactions all employ one or more of the following terms: electron bunching, linear velocity modulation, angular velocity modulation, and phase focusing [6]. Bunching refers to creating higher density groups of electrons as in triode vacuum tubes [1]. Linear velocity modulation refers to changing the electron energy along the propagation direction of the electron beam as in a linear beam device

CONTACT Claudio Paoloni c.paoloni@lancaster.ac.uk Engineering Department, Lancaster University, Gillow Avenue, LA1 4YW, Lancaster, UK

while angular velocity modulation refers to changing the energy of electrons azimuthally in a plane perpendicular to a steady magnetic field as in gyro-devices. Phase focusing refers to increasing or decreasing the coupling of electrons according to their positions and drifts as in M-type (crossed field) devices and peniotrons.

In linear beam devices, electrons amplify rf fields through loss of kinetic energy. In these devices, an electron stream, formed and accelerated by an electron gun, is injected into an interaction region. Here, while drifting in relatively rectilinear motion, the electrons form bunches in the retarding field of a wave which is on, or inside, a nearby structure. As the electrons give up energy, the rf wave amplitude increases.

Perhaps the most successful microwave and millimeter wave amplifier has been the traveling wave tube (TWT). In traveling-wave tubes (TWTs), the electron stream moves in the field of a traveling electromagnetic wave whose phase velocity is slowed to the beam velocity by e.g. helices, coupled cavities, or ring bar and ring loop. When the velocities are approximately equal, the rf wave amplifies.

The paper aims to be a comprehensive review of the state of the art of millimeter wave TWTs, with a mention to Backward Wave Oscillators (BWOs) that belongs to the TWT family.

The paper starts with the description of the main applications of TWTs followed from an overview on the working mechanisms. The historical evolution of TWTs from helix to more advanced configuration is introduces. A section on advanced fabrication technology will inform on the fabrication challenges of millimeter wave TWT. Finally, a review of the main interaction structures will be proposed, supported by the most interesting examples of fabricated millimeter wave TWTs.

2. TWT applications

Although the TWT was invented by Kompfner in 1942, this device remains an integral constituent of satellite communication systems, electronic countermeasures, and radar systems [7–11]. The success of TWTs can be attributed to their wide instantaneous bandwidth (greater than three octaves have been achieved in some devices), high gain (up to 70 dB), and light weight (typically 2–200 lbs.). Operating frequencies are typically from 1 to 200 GHz with pulsed power levels in the 0.1–3 MW range (nominal 10% duty) and CW levels in the 10 W–20 kW range. As noted later, modern fabrication techniques have extended their operating frequency regime to 1 THz.

The output power TWTs can provide is at least one or two orders of magnitude higher than any existing solid state power amplifier. This makes TWTs the enabling devices for a number of fundamental applications, mentioned above. So far, TWTs at frequency higher than 90 GHz are not yet in the market, but their availability will permit a number of new applications.

Transmitters in satellite communications systems are mostly powered by TWTs. In addition to the high power, TWTs are relatively unaffected by radiation and harsh thermal conditions, making them highly reliable as required in the space environment. Currently, the maximum operating frequency for space TWTs is about 70 GHz. However, it is already envisaged the use of E-band (71–86 GHz) for very high data rate satellite communications [12].

The use of TWTs in wireless communications is gaining interest for the opportunity to exploit the spectrum above 90 GHz. More than 100 GHz bandwidth is available between

90 and 300 GHz. This permits 10s gigabit per second data rate. The main obstacle for the use of this frequency range is the high atmospheric and rain attenuation and the available transmission power of millimeter solid state devices that limits the transmission range to very short distance or needs very high gain antennas, with significant difficulty of alignment and sway. The development of wireless systems based on the use of TWTs are in progress for enabling point-to-multipoint, multigigabit per second data distribution that will provide an affordable replacement of fiber over wide areas, with substantial cost reduction.

Plasma diagnostics of microturbulence in nuclear fusion reactors is an application that would benefit from the availability of high power THz sources. The nonperturbative diagnostic is based on collective Thompson scattering. So far, only bulky and low power laser sources are available. Backward wave oscillators are the ideal radiation source for this application. An international collaboration is working to produce a 0.346 THz BWO [13].

A possible application of TWTs is in imaging. The wide band and high power at millimeter waves permit high resolution and stand-off imaging. A novel application where TWTs are pivotal is the ViSAR (Video Synthetic Aperture Radar) at 235 GHz [14]. It is able to penetrate clouds and works in all-weather conditions providing high resolution imaging. A TWT with 50 W of average power at long duty cycles across the entire band of operation is used [14].

TWTs are also the power amplifier of a wide range of electronic countermeasures, typically at frequency below 40 GHz.

TWTs are enabling amplifiers for well-established and future applications, making possible the exploitation of the millimeter wave spectrum.

Figure 1 shows the broad range of performance achievable by TWTs and other vacuum electron devices up to 300 GHz. It demonstrates the relevance of TWTs as enabling devices for the applications described.

New fabrication tools and technologies as well as modeling tools and new applications are fueling a renaissance in high frequency TWTs and BWOs.

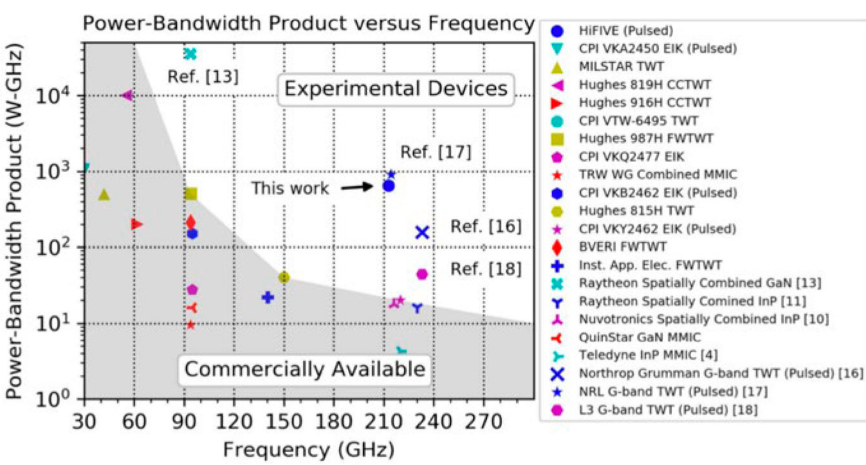


Figure 1. State of the art for TWT performance [15] (references in the figures can be found in the original paper).

3. Physical mechanisms of TWT operation

A simple picture of TWT amplification is obtained by considering a group of electrons approaching a retarding field. The electrons will lose kinetic energy and gain potential energy, thereby adding energy to the retarding field. If the electron density increases sufficiently during this process, the space charge fields also add to the retarding field. In a TWT, groups of electrons undergo similar energy changes in the retarding portion of an RF field traveling inside the device. This leads to amplification of the RF field.

To better understand the physical picture of the TWT interaction, consider Figure 1. which illustrates the case of a wave propagating along a helix through which an electron beam is assumed to propagate. Although the wave propagates at essentially the speed of light along the helix, its effective forward velocity is sufficiently slow (as determined by the helix pitch) to synchronously interact with the electron beam traveling at $u_o \approx 0.1c$. Figure 1 also schematically illustrates the variation in the axial electric field strength of a continuous bunching process. Due to the negative charge of electrons, positive (negative) E_z results in a force to the left (right). This leads to bunching about the positions indicated by B in Figure 2. This also leads to a larger number of electrons in the region of the decelerating fields (position B) as compared to the accelerating field.

At the entrance to the helix, the electrons have a drift velocity slightly greater than the phase velocity of the rf wave and bunch near the nodes of the electric field. The electrons traveling through the helix continuously drift toward the decelerating electric field, causing an increase in wave amplitude. As the field amplitude increases, the bunching process becomes stronger leading to a reinforcement in wave amplitude and exponential growth below saturation.

As we shall see in the following, there are currently two major types of traveling wave tubes in active use: helix TWTs and coupled cavity TWTs, although a variety of other circuits

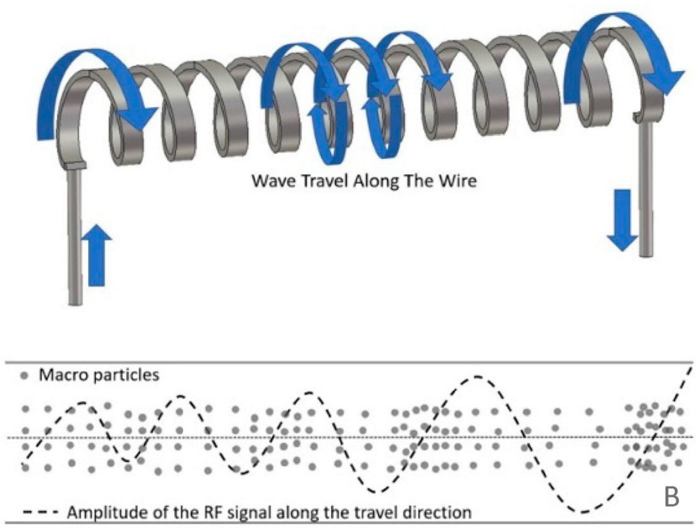


Figure 2. Schematic illustration of the interaction between an electron beam and a wave propagating along a helix.

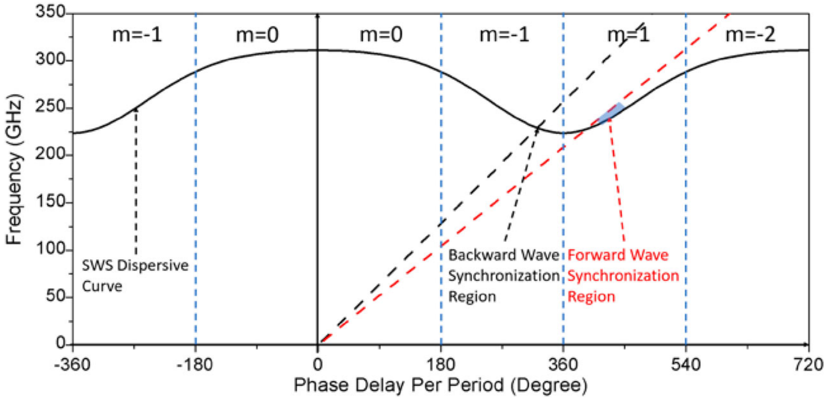


Figure 3. Schematic illustration of the dispersion relation for a slow wave circuit.

such as folded waveguides, corrugated waveguide, ring-bar, grating, and ladder configurations are either employed in specialized applications or are under investigation for millimeter wave TWTs. [16–21] The former has essentially continuous interaction while the latter has interaction only in the cavity gaps. In all cases, the slow wave circuit has a phase velocity less than the velocity of light in order to synchronously interact with the electron beam and is a forward wave (phase and group velocity in the same direction as shown in Figure 3). Figure 4 displays sketches of commonly employed slow wave circuits in commercial TWTs. The particular choice of SWS depends upon a number of criteria including operating frequency, bandwidth, peak and average output power, and gain. The broadest bandwidth is obtained with the helix SWS, particularly with the use of so-called "dispersion shaping" [22,23]. As it will discussed in the following, unfortunately, helix SWS cannot be used above 60–70 GHz due to difficulty of fabrication.

The application of the above criteria to the tape helix structure reveals a number of its natural advantages. Perhaps the most important advantage of the helix structure lies in its broad bandwidth which is due to the low dispersion of the circuit. This property is essential to its use in communications and electronic countermeasures (ECM) applications as well as wide bandwidth laboratory amplifier usage.

There are several reasons which lead to the power limitations of helix tubes. The small heat capacity of the structure provides a significant limitation on the power handling capability. However, there are additional constraints which should be understood. First, we must employ electron beams which only partially fill the helix tunnel in order to help suppress backward wave oscillations [24]. This, therefore, results in a limitation on beam current due to space charge forces for a given beam voltage. Simply increasing the beam voltage is not a viable solution since this requires that the helix pitch angle be increased to maintain synchronism. This results in a decrease in the interaction impedance for the forward mode thereby decreasing the efficiency. In addition, the relative impedance at the spatial harmonic is increased, thereby leading to increased susceptibility to backward wave oscillations. Consequently, most helix tubes have tended to operate with beam voltages of < 10 kV. Although limited in power output capability, the helix TWT plays an important role in many applications, particularly telecommunications where the development history is

Table 1. Representative performance characteristics of space TWTs.

Band	Output Power	Approx. Efficiency	Approx. Mass	Manufacturer
X-band (8–12 GHz)	100–160 W	64–69%	1250 g	L-3
Ku-band (12–18 GHz)	35–205 W	60–71%	695 g	L-3
K-band (18–27 GHz)	150–300 W	63–68%	1400/1700 g	L-3
K-band (18–27 GHz)	160 W	63%	900 g	Thales
Ka-band (27–40 GHz) Q-band (33–60 GHz) V-band (40–75 GHz)	10–200 W	30–60%	1500 g	L-3
Q-band (33–60 GHz)	40 W	50%	950 g	Thales

reviewed in [7]. Table 1 displays typical parameters of helix TWTs used for satellite down-link applications.

Here, it should be noted that approximately 90% of the world market is shared between L-3 Harris (US) and Thales (France).

An interesting usage of helix TWTs has been in the so-called microwave power module (MPM) and millimeter wave power module (MMPM) [25]. This hybrid device combines the best features of solid-state device technology with that of vacuum electron devices. Specifically, the MPM consists of a low noise, solid-state MMIC preamplifier, a TWT vacuum power tube booster, a solid-state equalizer, and integrated power conditioner (IPC). Here, the solid state device provides the low noise input and initial gain while the TWT provides the final 20 dB gain. The small size and light weight have facilitated numerous applications including drone based systems. The development of the approach has moved from the 2–18 GHz microwave region to the upper millimeter wave region up to G-band (230 GHz) [26]. Table 2 below displays the performance characteristics of most relevant MMPMs.

As mentioned in the preceding, the helix structure is not suitable for high power operation due to its limited heat dissipation capability. In addition, the high beam voltages required for high power tube operation result in the evolution of the helix to a more open structure. Consequently, an increased fraction of the field energy is stored in high order spatial harmonics thereby degrading the interaction efficiency. The concomitant reduction in impedance and propensity toward backward wave oscillations lead to serious operating difficulties although some techniques such as the use of resonant loss have led to stable operation at increased beam voltage and power [33]. Using such techniques and modern computational tools, it has been possible to increase the operating voltage to $\sim$17–20 kV and the output power of K/Ka band and Q-band helix TWTs to the hundreds of watt level [34–37]. The above limitations motivated the development of so-called helix derived circuits (see Figure 2) which partially ameliorate the situation, albeit at a cost in bandwidth among other problems. The ring-bar circuits tend to produce higher power (up to 200 kW peak and 10 kW average in UHF and L-Bands) with kW levels obtained at Ka-band [38]. Here, the phase velocities considerably exceed those of the simple tape helix with up to $\approx$ 0.4–0.5 *c* (where *c* is the velocity of light).

A related interaction structure is the Tunnel Ladder circuit [39,40] which grew out of the Karp Circuit [37–42] which is a ridged waveguide whose broad wall contains an array of transverse slots. In the baseband of this circuit, the electrons alternately see a strong field and a weak field as they pass, respectively, over a slot and over the metal between the slots, making spatial harmonic operation possible.

Table 2. Performance characteristics of MMPMs.

	Ka Nano [27]	Ka Band [28]	Dual Ka/Q [29]	Q Band	Multi-Band [29]	E Band [30]	Pulsed W Band [31]	W Band [32]	G Band [15]
Frequency (GHz)	29–31	26– 40	29.5–31 43.5–45.5	43.5–45.5	18–40	81–86	92–96	91–97	231–235
Output Power (W)	50	50	80	80	100	100(sat)/ 50(lin)	100	50(min)	32
Volume (cm^3)	16.6 × 10.4 × 2.5 cm	24.1 × 20.3 × 3.8 cm	24.1 × 20.3 × 3.8 cm	24.1 × 20.3 × 3.8 cm	24.1 × 20.3 × 3.8 cm	37.6 x 26.7 x 7.6	37.5 x 21 x8	39 x 18 x4.5	38 x 24 x 7
Weight (kg)	1.1	3.9	3.9	3.9	3.9	10.	10.4	6	9

The concomitant reduction in impedance and propensity toward backward wave oscillations lead to serious operating difficulties for the tape helix TWT which were only partially ameliorated by the helix-derived circuits. This, therefore, led to the development of coupled cavity slow wave tubes shown schematically in Figure 4 and which comprise the majority of current high power tubes despite their relatively narrow bandwidth. Basically, these can be thought of as derivations from series lumped LC element bandpass filters. The coupled cavity structure possesses a number of attractive attributes. Of particular importance is the fact that the radial heat conduction is greatly facilitated by the metal webs which serve as the cavity walls. In addition, the shape of the structure is quite compatible with periodic permanent magnet (ppm) focusing and the assembly, although tedious, is relatively straightforward due to the symmetry. Finally, although inferior to the helix structure, coupled cavities provide moderate bandwidth ($\sim$ 2%–30%) as well as reasonable interaction efficiencies and mode structure.

Coupled cavity TWTs (CCTWTs) have found service in the 1–100 GHz region with the lower limit set by the availability of alternative sources which are more cost effective. The upper limit is primarily set by machining and fabrication difficulties. As an example of the dimensions involved, the beam hole diameter in a 94 GHz tube is $\sim$ 0.508 mm which is to be compared to the 0.1524 mm diameter of a human hair. Therefore, this necessitated the development of manufacturing processes which maintained tolerances of a few microns for the success of the early millimeter wave CCTWT developments. Bandwidths of coupled cavity tubes range from the order of a few percent up to $\sim$ 43%. However, as we shall see, attaining bandwidths of even 30% requires a number of design compromises. Peak powers have ranged from $\sim$ 100 W to 0.5–10 MW [43,44]. The latter is not a hard limit and has resulted somewhat from the fact that the applications requiring high power have been able to be satisfied using narrowband amplifiers such as klystrons. Beam voltages have tended to be in the range of 8 kV to 85 kV. The lower limit arises because the cavity period decreases with decreasing beam voltage. The high frequency limitation arises both because the bandwidth decreases with increasing beam voltage and also because many applications preclude the use of high voltage. Finally, saturated tube gains up to $\sim$ 60 dB are typical. This could be further increased, if necessary, by increasing the number of gain sections from the present three to four although the possibility of external feedback induced oscillations would also be increased.

The peak power limitation in coupled cavity tubes depends somewhat upon the space harmonic used for operation. Lower space harmonics require higher beam velocities to achieve synchronism and generate higher interaction efficiencies because of their higher interaction impedance. Since higher beam velocities also typically permit higher output powers, CCTWTs operating in a forward fundamental mode are found to produce powers about an order of magnitude above the peak powers from CCTWTs operating in a forward

Table 3. Operating characteristics of currently available coupled cavity TWTs.

Frequency Band	Operating Freq.	Power	Duty	Manufacturer
W-band	93–95 GHz	50 W	CW	CPI
W-band	95–96 GHz	3 kW	10%	CPI
Ka-band	34.5–35.5 GHz	50 kW	30%	CPI
Ka-band	30–31 GHz	500 W	CW	CPI
Ku-band	16–17 GHz	50 kW	0.3%	L-3

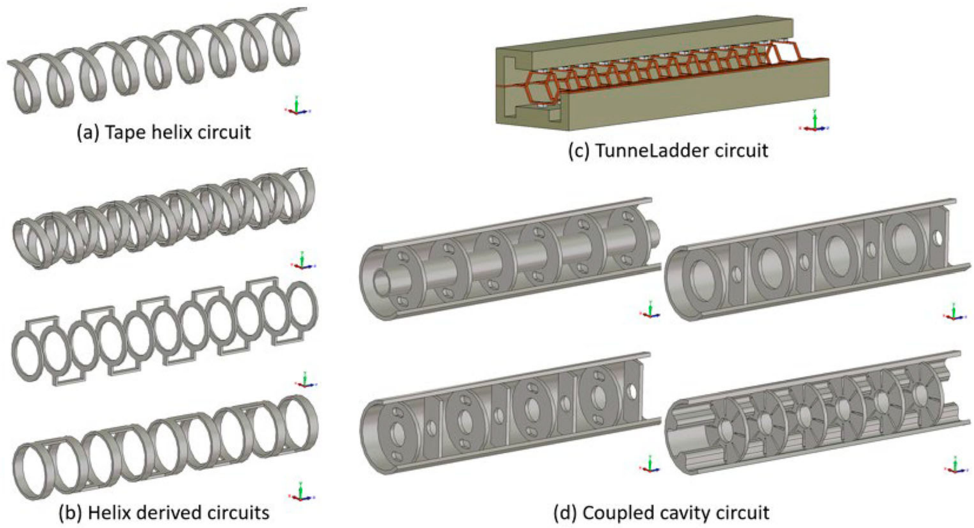


Figure 4. Common commercial TWT slow wave circuits.

first-space-harmonic mode. At X-band, a 500 kW cloverleaf TWT [45] and a 1.2 MW centipede TWT [46] with high power, X-band tubes which produce between 100 and 125 kW (as also advertised in older sales brochures of Hughes Aircraft Co., Litton Industries, and Varian Associates). Table 3 displays the operating performance of representative currently available coupled cavity TWTs (Figure 4).

4. Backward wave oscillators operation and state of the art

Backward wave oscillators (BWOs) are similar to the TWTs discussed in the preceding section in that they employ a slow wave structure and a traveling wave interaction. However, they differ in one major respect. Specifically, the electrons interact with a backward wave rather than a forward wave (see Figure 3). As we shall see, this makes possible the operation of extremely broadband voltage tuned oscillators. A simple physical picture indicating the mechanisms responsible for the internal feedback of the BWO was developed by Heffner [47] and is illustrated in Figure 5. Here, an electron beam is assumed to propagate at near the synchronous velocity close to the surface of a slow wave structure which supports a backward wave. The direction of phase advance of the wave is taken to be that of the electron beam propagation direction so that the energy flow on the circuit is opposite the beam drift. As with the TWT, the electric field of the circuit wave causes a velocity modulation of the beam electrons. Following a phase delay of $\pi/2$, this manifests itself as a current modulation which undergoes a phase delay of $\beta_e L$, where β_e is the beam propagation constant as it travels a distance L equal to the circuit length. An additional phase delay of $\pi/2$ occurs as the current modulation excites the circuit electric field. Energy propagation along the circuit then undergoes a phase advance of βL due to the backward wave nature of the wave. In order to have feedback oscillations, one requires an integral multiple of 2π for the phase shift.

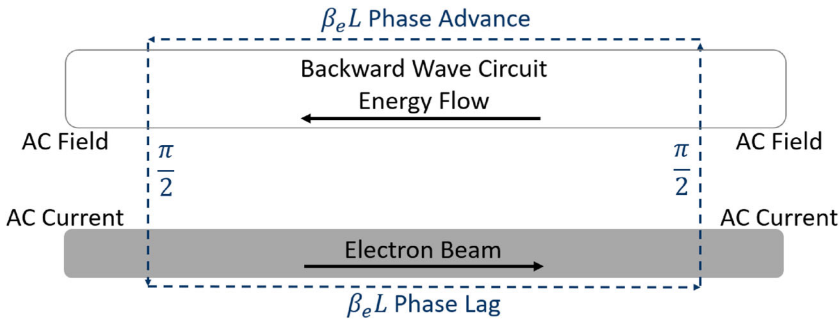


Figure 5. The feedback loop of a backward-wave tube.

Historically, these devices have found extensive application as low to moderate power ($\approx$ 1–300 mW) swept sources from the microwave to submillimeter wave region. There are both crossed field BWOs (sometimes referred to as M-type) and linear beam BWOs or O-type BWOs. Since the majority of the millimeter wave devices currently in use are of the latter type, the discussion shall be primarily restricted to them. These are also sometimes referred to as carcinotrons which was the trade name for BWOs manufactured by Thomson – CSF (In December 2000, renamed Thales). There are a number of excellent references concerning the principles of operation of BWOs as well as their design. The text by Gewartowski and Watson [1] provides a sound foundation for calculating BWO start oscillation and the connection to the TWT formalism described in the preceding subsection. Theoretical analyses of BWOs including start oscillation and efficiency calculations may be found in the papers by Heffner [47]; Johnson [48]; Grow and Watkins [49]; and Karp [50]. Construction details and performance data for some early BWOs operating in the 1–12 GHz region are provided in the paper by Palluel and Goldberger [51]. Information concerning millimeter wave BWOs can be found in the chapter by Kantorowicz and Palluel [52]. In addition, an excellent discussion of high power millimeter wave BWOs is contained in the chapter by Forster [53].

For many years, a major market for BWOs was in laboratory sweep oscillators up to 200 GHz. However, advances in solid state technology including active amplifiers and frequency multipliers have essentially eliminated that market. What remained was service as local oscillators in submillimeter wave astronomy, spectroscopy instruments, and as swept probe sources in plasma diagnostics [53–64].

Throughout the years up to 2000, the two main producers of BWOs were Thomson-CSF in France and Istok in Russia with tubes operating up to 1 THz, albeit at relatively low power (mW to W depending on frequency) with limited lifetime (200–2000 hrs.). The Thomson-CSF tubes employed a vane type circuit [51,54,65]. The major problem with the vane type circuit is that the fundamental mode is a forward wave. The forward wave nature of the circuit necessitates operation with the first spatial harmonic with its attendant sharply reduced interaction impedance leading to higher required beam voltages and reduced efficiency. However, this shortcoming was in large part offset by the ease of machining fabrication and inspection for the vane structure. Figure 6 displays the output power versus operating frequency for the Thomson-CSF family of millimeter wave BWOs. Here, it is useful to review the features of the 1 THz tube which reveals the challenges and limitations also relevant for

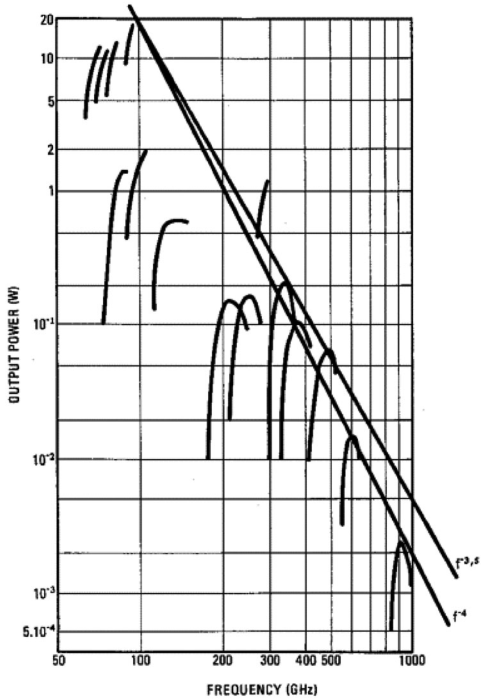


Figure 6. Output power versus frequency for Thomson-CSF MMBWO family [54].

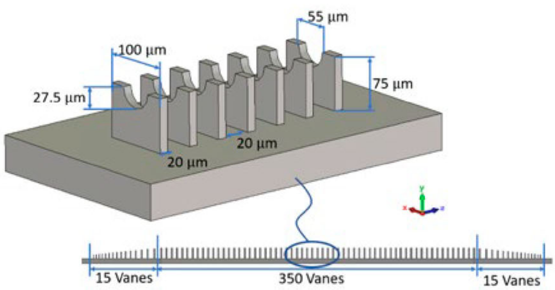




Figure 7. Vane type slow wave structure for 850–1000 GHz Carcinotron [65].

TWTs at the same frequency [54]. The vane type slow wave structure is shown in Figure 7 for the 1 THz Carcinotron.

The THz carcinotron employed the same basic fabrication and design techniques as their preceding tubes although severely pushing the limits of the technology of the time [66]. This tube utilized a 500 µm diameter M-type cathode with the cathode emission densities potentially reaching 18 A/cm^2. However, some of the emission appeared to come from the edges and sidewall of the cathode thereby relaxing this number somewhat. Using an 8 kG $SmCO_3$ magnet system, the electron beam was compressed to 50 µm diameter for passage through the 55 µm beam slot shown in Figure 7. The cathode voltage was designed to vary between 4 and 10 kV over the operating frequency range of the tube. As shown in Figure 7,

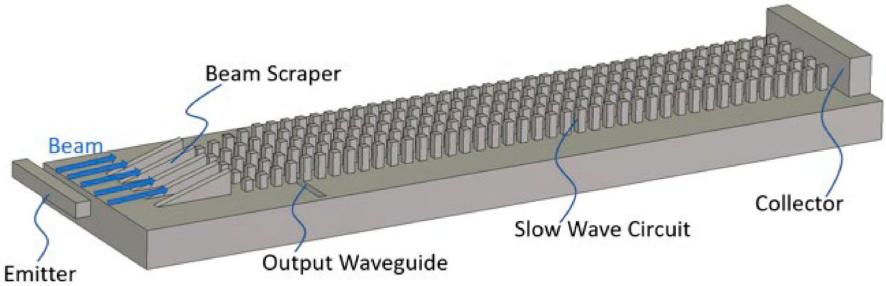


Figure 8. Istok submillimeter wave BWO schematic.

the slow wave structure consisted of 350 vanes of uniform height with 15 vanes at both the input and output ends serving as matching sections. For comparison purposes, the lower frequency tubes had uniform sections of 200 vanes. The slow wave structure was milled out of copper using a 20 μm cutting wheel.

THz BWOs were also developed by the Istok company in Russia and are still produced and sold [67]. As shown in Figure 8, the approach differs from that adopted by Thomson-CSF. Here, instead of a circular cathode and large compression ratio, a rectangular cathode operating at high current density produces an electron beam which passes through a beam scraper which carves out the portion of the electron beam which would otherwise impinge upon the fragile slow wave circuit pintles. In the simplest embodiment, there is no beam compression thereby requiring cathode current densities as high as possible consistent with acceptable, albeit limited, lifetime. Figure 9(a) displays the Istok submillimeter wave BWO performance characteristics with a photograph of the 900–1100 GHz shown in Figure 9(b).

As noted in [67], the demand for, and hence development activity on, high frequency BWOs, similar statements apply to the Thomson-CSF carcinotrons, has significantly declined. This is attributable to the size and weight of the magnet, power consumption, lifetime, and the challenges in fabricating such tiny and delicate structures with the tools previously available.

4.1. Millimeter wave and THz TWTs

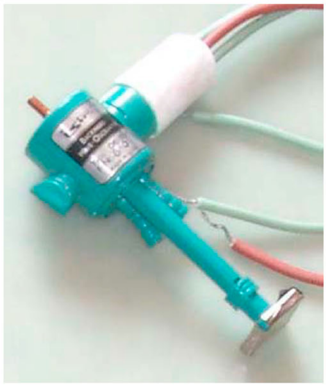
The evolution from helix TWTs to new concept TWTs at millimeter waves is fostered by the use of new technologies and processes. The substantial amount of research and production of microwave TWTs described in the previous sections has been a fundamental stage for their evolution. The scope of this section is to describe the latest advancements in TWT technology.

Manufacturing processes have to respond to the accuracy and dimensions that the short wavelength at millimeter wave frequency require. Electron optics need a miniaturization approach to assure electron beams are of small diameter and well confined.

Slow wave structures (SWSs) have to assure the best beam-wave interaction with dimensions dictated by the wavelength and fabrication technologies. The most relevant millimeter wave SWSs and their implementation in TWTs, applicable also to BWOs, will be discussed.

Model	OB-65	OB-67	OB-80	OB-81	OB-82	OB-83	OB-84	OB-85
Frequency band, GHz	258-375	370-535	530-714	690-850	790-970	900-1100	1070-1200	1170-1400
Minimal output power, mW	1-10	1-5	1-5	1-5	0.5-3	0.5-3	0.5-2	0.5-2
Voltage, kV	1 - 4	1 - 4	2 - 6	2 - 6	2 - 6	2 - 6	2 - 6	2 - 6
Current, mA	25-40	25-40	30-45	30-45	30-45	30-45	30-45	30-45
Magnetic field, kOe	7	9	10	10	11	11	11	11

a)



b)

Figure 9. (a) Istok submillimeter wave BWO performance characteristics (b) Photograph of Istok submillimeter wave BWO OB-83 (frequency band 900-1100 GHz, mass < 250 g) [67].

4.2. Microfabrication technologies

One of the reasons for the slow development of mm-wave TWTs is the fabrication challenge that interaction or slow wave structures pose. The scaling down of dimensions at the increasing frequency brings the dimensions to the limit of conventional machining. High tolerance, extreme surface finishing, and flatness are only some of the parameters that have to be ensured for a high quality fabrication. As described in the following, most of the SWSs at millimeter waves have to be built in two halves, adding a further challenge in high precision alignment.

In the following, the principles of the most common microfabrication processes used for SWSs production are described. Further details can be found in the literature [68].

4.2.1. LIGA

LIGA is a German acronym for Lithographie, Galvanoformung, Abformung (Lithography, Electroplating, and Molding) [69]. It is a lithographic microfabrication process based on the use of thick photoresists (SU-8, PPMA, or KPRM) that produce high aspect ratio molds for growing copper structures by electroforming.

The LIGA process permits one to obtain sizes of features not achievable by CNC milling or other techniques, with high quality surface finishing.

Two different LIGA processes are available depending on the size of the minimum features: Deep X-ray LIGA (PPMA) and UV-LIGA (SU-8, KRPM) [70].

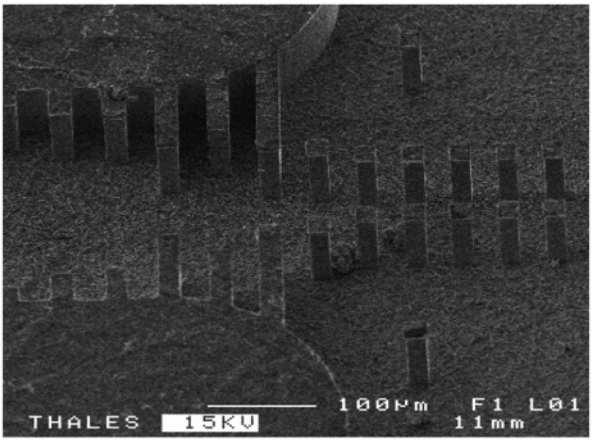


Figure 10. Detail of DCW at 1THz realized by Deep X-ray LIGA. Pillar section is 20 × 20 microns, height 70 micron [70].

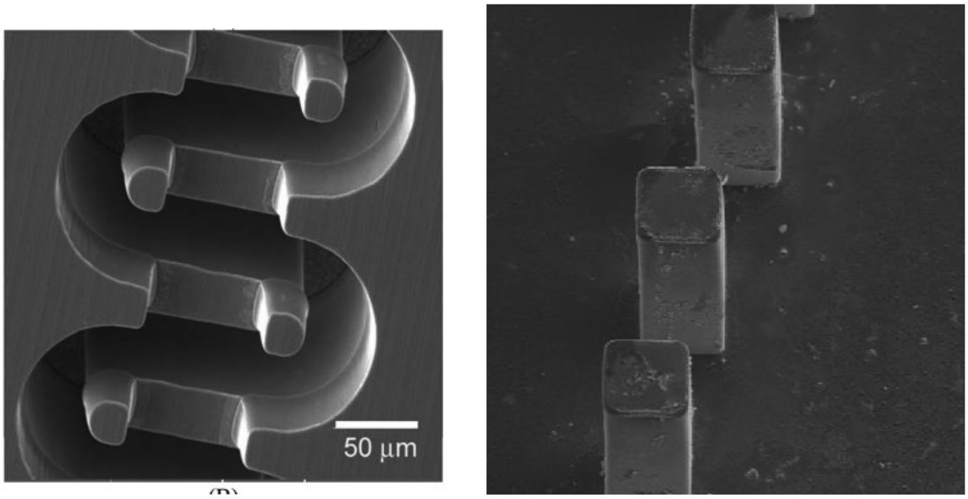
Deep X-ray LIGA uses metal masks and PMMA (Poly(methyl methacrylate)) photoresist exposed to X-rays produced by a synchrotron light source. Aspect ratios up to 100:1 can be achieved. The first double corrugated waveguide at 1 THz realized by Deep X-ray LIGA is shown in Figure 10. The pillar section is 20∗20 microns and the height is 60 microns [70]. The process is quite expensive and not widely available since it requires a synchrotron light source.

UV-LIGA, in contrast to Deep-X-ray LIGA, is an affordable process. The resist is exposed by an ultraviolet (UV) light available in normal mask aligners. Two different photoresists can be used, SU-8 and KMPR. SU-8, surely the most widely used for millimeter wave SWSs, provides higher quality molding, but it is very difficult to remove at the end of the process. KMPR is easier to remove, but it is limited in the achievable aspect-ratio. The maximum aspect ratio allowed by UV-LIGA is about 20:1, sufficient for most of the SWSs. Two examples of UV-LIGA SWSs are shown in Figure 11(a) shows a 1 THz folded waveguide [71,72], while Figure 11(b) shows the pillars of a 300 GHz double corrugated waveguide [73] (the pillar section is 70 × 70 microns).

Note the high quality of the metal surfaces. Other examples of LIGA fabrication are reported in [74–78] including the SU-8 removal process, and cold tests on different slow wave structures in the millimeter wave band.

4.2.2. High precision CNC milling

CNC (Computer Numerical Control) milling is the typical fabrication technique for metal parts. However, when the size of the features, as in millimeter wave SWS, approaches the 100 micron level and the surface roughness needs to be in the range of tens of nanometers, the process become very challenging and high end equipment is needed. The quality of fabrication is a function of the accuracy and resolution of the positioning and the availability of suitable toolings and high spindle speed (higher than 20,000 rpm) [79–83]. High-end CNC mills available in the market provide resolution of about 100 nm. At the top of the scale, there is the DMG Mori Seiki NN1000 developmental nano-CNC mill, available at the University of California Davis, that has a movement position accuracy of 1 nm/100 mm



a) b)

Figure 11. (a) 0.67 THz folded waveguide [72]; (b) 300 GHz double corrugated waveguide (pillars section 70 × 70 microns) [73].

and a repeatability of 5 nm/100 mm. The spindle currently employed in the machine has a maximum speed of 50,000 r/min [80].

Tooling are of high importance for the size and the quality of the surfaces. The most suitable for high precision machining are coated carbide and diamond tooling. The minimum size available is 76 um diameter, that poses substantial material and use challenege.

Nano-CNC milling has been demonstrated able to produce SWSs up to 0.346 THz (Figure 12). The shown 0.346 THz double staggered grating structure is surely close to the limit of the CNC milling technology. It consists of two identical halves that have to be assembled with high precision alignment.

Commercial high end CNC milling is also used for SWS at lower frequency that do not need the level of accuracy above described.

Figure 13 shows two SWSs produced by a commercial high speed CNC milling (Primacon) with better than 1 micron accuracy. Figure 13(a) shows a 92–95 GHz folded waveguide,

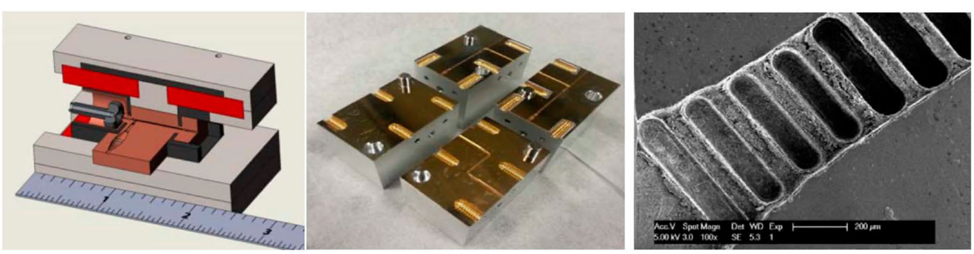


Figure 12. Detail of 0.346 THz Double Staggered Grating (a) 346-GHz compact BWO shown with 6-in ruler for scale. (b) Cold test circuit structures. (c) SEM image of the DSG circuit cavities.

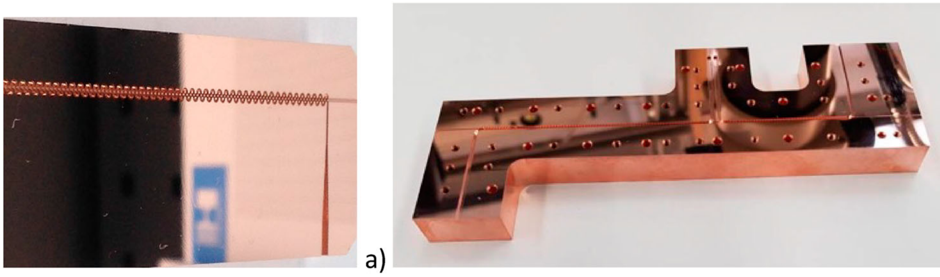


Figure 13. (a) High precision CNC milling (a) W-band Folded Waveguide [82] and (b) D-band double corrugated waveguide [83].

specifically one of the two identical halves that once assembled formed the closed waveguide [82]. Figure 13(b) shows a 140 GHz double corrugated waveguide [83].

4.2.3. Micro diffusion bonding

The fabrication of the parts is the first step of the full fabrication process of a SWS. As mentioned above, millimeter wave SWSs are usually built in two halves to be assembled. The assembly has to be vacuum tight to maintain the high vacuum level needed for the functioning of the TWT (better than 10^{-8} Torr). Diffusion bonding is a process that permits one to assemble two or more metal parts by rebuilding the atomic bonding at the contact surface [84]. This is achieved by applying a high pressure to the two halves to assemble by a specific holder. The holder is then baked at a temperature close to the melting point of the metal. The combination of temperature and pressure recreates the atomic bonding between the contact surfaces. The resulting bond is vacuum tight.

4.3. Electron optics

The electron optics is the subsystem that permits the generation and collection of a confined electron beam with given shape and electrical parameters. The electron optics include the electron gun, the magnetic focusing system, and the collector. In this section, only the electron gun will be discussed since it is the most complex constituent of the electron optics and linked to the TWT performance. Details on the magnetic focusing system and collector can be found in literature.

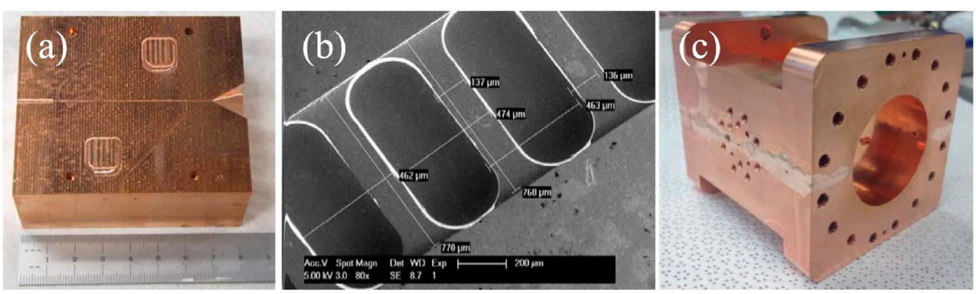


Figure 14. Example of circuit blocks and diffusion bonding: 220-GHz DSG [81].

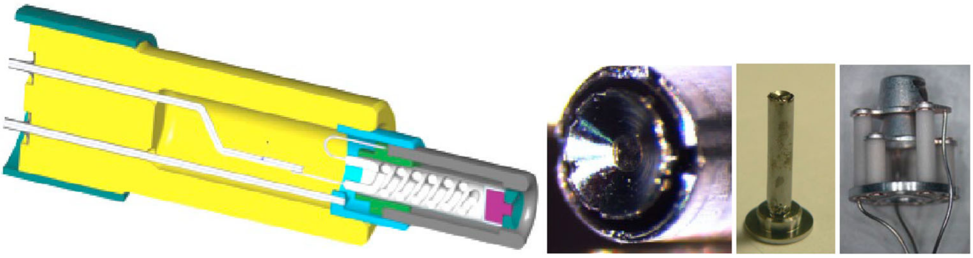


Figure 15. Schematic and parts of an electron gun for 1 THz BWA [70].

The Pierce electron gun is the most used configuration, built to generate a cylindrical electron beam to interact with a helix SWS. It has been demonstrated to be suitable to produce electron beams with 20 micron radius (Figure 15) [70]. The focusing of cylindrical electron beams is well established by using periodic permanent magnet systems.

Recently, in response to the use of slow wave structure with a wide interaction field distribution, and the need to increase the current while maintaining a low current density, electron guns to produce electron beams with rectangular section (sheet electron beam) were realized (Figure 16).

The advantage of sheet electron beams is their wider cross section that well matches the field distribution in corrugated "like" SWSs, usually distributed over a wide region closed to the corrugations. The main challenge of a sheet electron beam is to design the magnetic focusing system. Sheet beams suffer the diocotron $\vec{E} \times \vec{H}$ effect, that brings a rotation of the beam and a critical level of impingement of electrons with the metal structure.

As the length of the beam transmission tunnel is increased, a periodic focusing magnetic field, rather than a uniform one, has been presented as a method to avoid kinking and filamentation instability [85]. Concurrently, by adopting a periodic permanent magnet (PPM) focusing system, the volume of the VED can shrink into the cm^3 range and the weight can be reduced to less than 10 pounds for THz frequency band operation. Previous work on this subject mainly focused on analytic studies to understand the interaction mechanism and theoretical modeling to design magnetic lens structures [86,87].

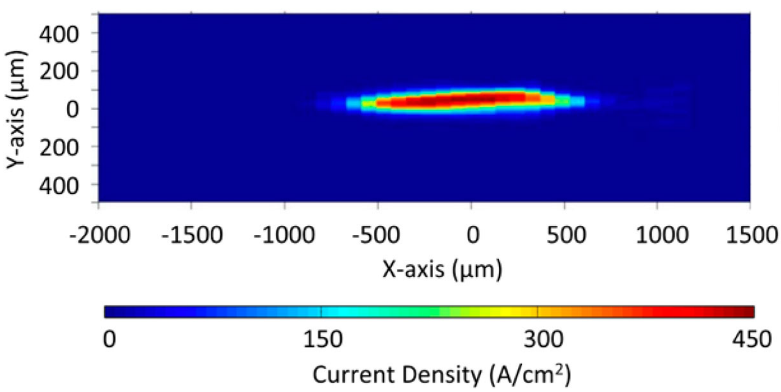


Figure 16. Measured beam profile for with the nanoscale tungsten scandate cathode. The measured aspect ratio is 12.5:1, the maximum current density (dark red color on this plot) is 438 A/cm [88].

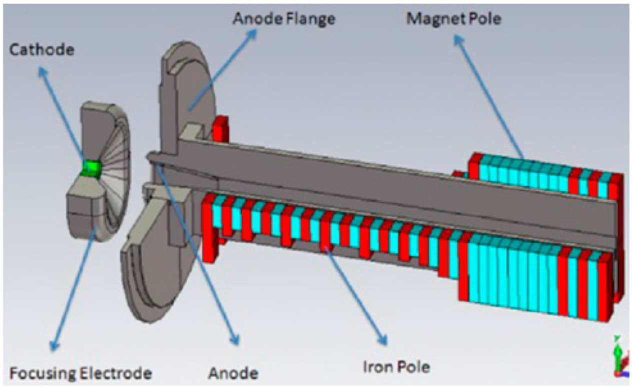


Figure 17. W-band sheet beam klystron (WSBK).

Several works related to the transport of gun-emitted sheet beams have been reported in recent years. An offset PCM structure developed by UC Davis has been employed in a W-band sheet beam klystron (WSBK) and the 90 A/cm^2 beam achieved 99% transmission with RF [89] (Figure 17). The focusing system for the WSBK is an offset periodic permanent magnet (PPM) which provides the appropriate vertical focusing force by periodic pole pieces and supplies the horizontal focusing force by the offset iron pieces.

The closed PCM focusing system adopts enclosed construction; it is rarely employed in high gain, moderate average power devices due to its restriction on space availability for the cooling channels of a liquid thermal management system. The traditional semi-open offset pole piece, periodic cusped magnetic (PCM) focusing system employed in W band tube sets the horizontal focusing magnet part at the fringe of the PCM poles. In addition, the width of the whole magnet is limited due to the requisite strength of the y-direction magnetic field. Consequently, the practical finite width of the traditional PCM will cause the tilt phenomenon in the beam mid-plane off the magnet array mid-plane which will deteriorate the beam transmission. A novel PCM-QM magnet has been presented to solve the abovementioned problems.

Figure 18 shows the transverse section and 3D beam transport model, including the main circuit block and the novel PCM-TQM structure, of the prototype 220 GHz / 263 GHz SBTWT amplifier [90]. This hybrid PCM-TQM focusing system can provide vertical direction (y-z plane) focusing by the PCM part and, simultaneously, confine the horizontal plane dispersion tendency of the sheet beam by the independent TQM part. Compared with the traditional PCM focusing system, the PCM-TQM focusing system has several advantages: First of all, this kind of PCM-TQM eliminates the width limitation of the traditional PCM focusing system by placing the TQM poles on the top/bottom surface of the PCM part. Consequently, this kind of system can be compatible with a wider PCM part. Secondly, since the sheet beam gun is usually designed with different compression ratios in the vertical and horizontal planes, this can cause the vertical and horizontal beam waists to occur at different axial positions. This advanced PCM-TQM focusing system can produce magnetic focusing field matching of the vertical and horizontal beam transport separately, since the TQM is independent from the PCM part. Finally, each independent QM stack can provide adjustment capability by sliding on the top face of the PCM part along the broken line, shown in Figure 18, which can provide the PCM-TQM the ability to match the transversal

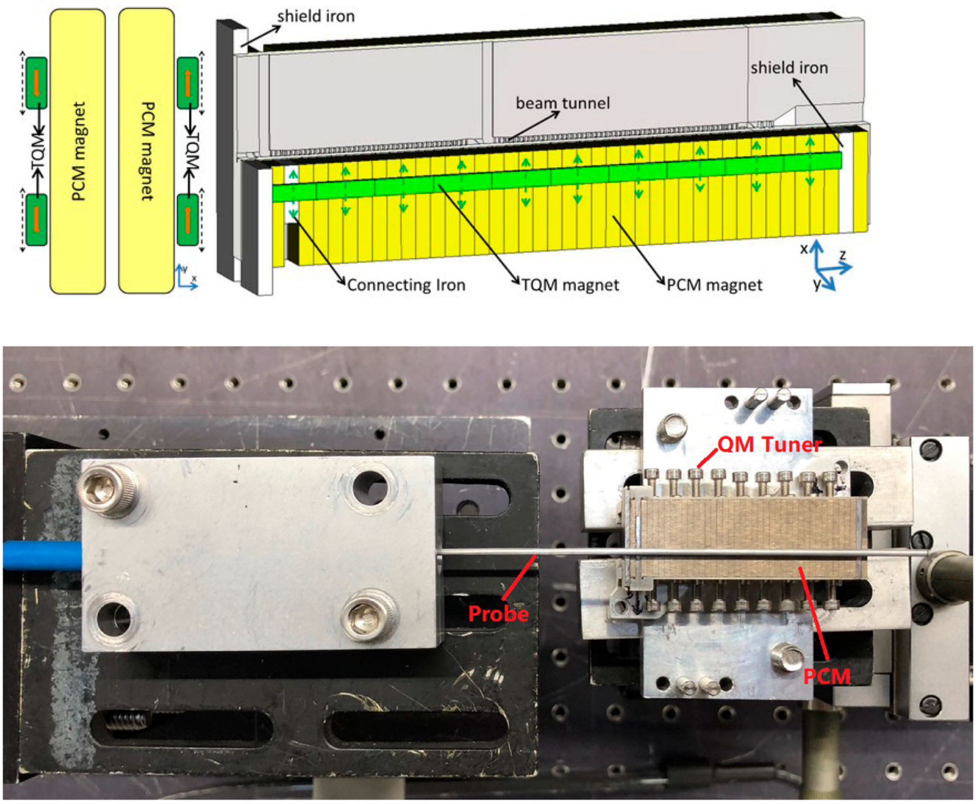


Figure 18. Transverse section and 3D beam transport model 220 GHz / 263 GHz SBTWT amplifier [90] schematic and fabrication.

focusing field with the varying beam current density. Furthermore, it provides the possibility of further adjustments to compensate for the inevitable magnet stack remanence variations and alignment issues after magnet assembly. Employing this PCM-TQM focusing system, the 263 GHz SBTWT achieves a 99.7% 'no RF' and a 97.6% 'with RF' beam transmission rate verified by CST-PS. Those results prove that this kind of structure has potential to benefit other sheet beam devices in the millimetre and sub-millimeter wave regimes.

4.4. Interaction structures for millimeter wave TWTs

Interaction structures or slow wave structures are the core of both TWTs, and similarly BWOs. They ensure the transfer of energy from the electron beam to the RF field. The quality of the energy transfer is measured by the interaction impedance [1].

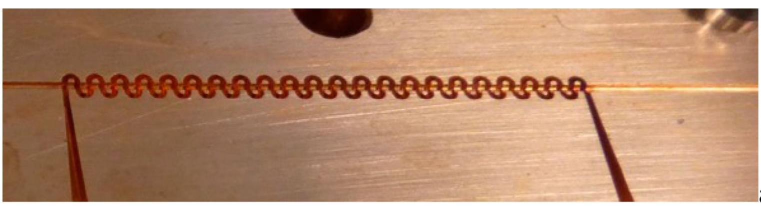
As discussed, helix and coupled cavity [2] SWSs typically used at microwaves have high interaction impedance. However, when the frequency increases above 60–70 GHz, the fabrication of those interaction structures is not feasible. Different interaction structures suitable for millimeter wave TWTs have been conceived to be fabricated with by the technology processes described in the previous section.

In the following, the most interesting interaction structures for millimeter wave TWTs, the folded waveguide, the double staggered grating, and the double corrugated waveguide, will be described including their application in state-of-the-art TWTs. Other SWSs have been proposed, such as meander lines [91–98] or planar helices [99], but no TWT was so far designed to be built, so they will be not considered in the following.

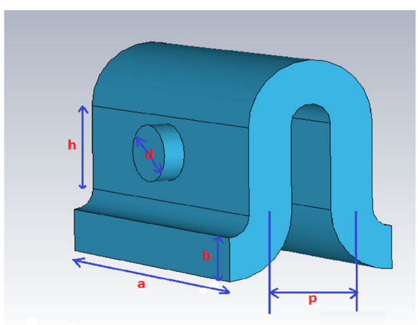
4.4.1. Folded waveguide

The folded waveguide (FWG) is a rectangular waveguide folded in a serpentine shape (Figure 19(a)) to reduce the axial phase velocity of the EM wave to have synchronism with the electron beam [100–102]. The single cell of an FWG SWS is shown in Figure 19(b). It consists of a bent waveguide with a circular beam tunnel. Compared with the helix slow wave structure, the FWG has narrower bandwidth, lower interaction impedance, but can provide higher average power handling capability since it is a full metal structure. The coupler to the flange is very easy to design with very good matching. The equivalent circuit model of the FWG SWSs is comparatively simple and the reflection in the structure is small. The Pierce gain theory [16] is a good approximation to predict the gain feature of the FWG.

In the attempt to improve the interaction impedance, some modified types of FWG SWSs have been proposed, such as the ridge-loaded FWG SWS (Figure 20) [103–108]. This topology has wider bandwidth, but also strengthens the longitudinal electric field thereby improving the electron efficiency of the beam-wave interaction. However, the complex geometric structure increases the manufacturing challenge at the increase of the frequency. To further simplify the fabrication of the FWG SWSs, and mitigate the ohmic losses, the Sine waveguide has been proposed for wideband, high-power terahertz TWTs (Figure 19(b)). It supports a sheet beam [109–113]. The interaction impedance of the sine waveguide SWS is low compared to a conventional FWG leading to a longer beam-wave interaction circuit, which will bring a challenge to the electron optical system.



a)



b)

Figure 19. Folded Wave Guide SWS (a) W-band copper sample, (b) schematic.

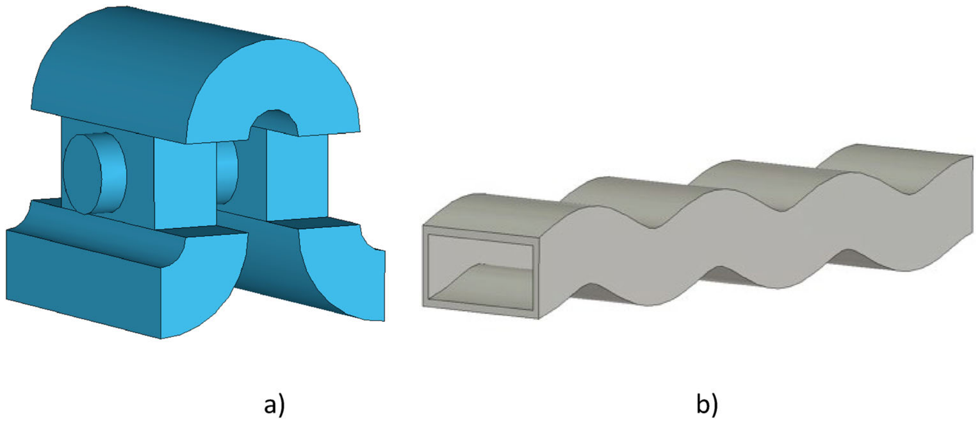


Figure 20. Modified FWG SWSs: (a) ridge-loaded [103]; (b) sine waveguide [110].

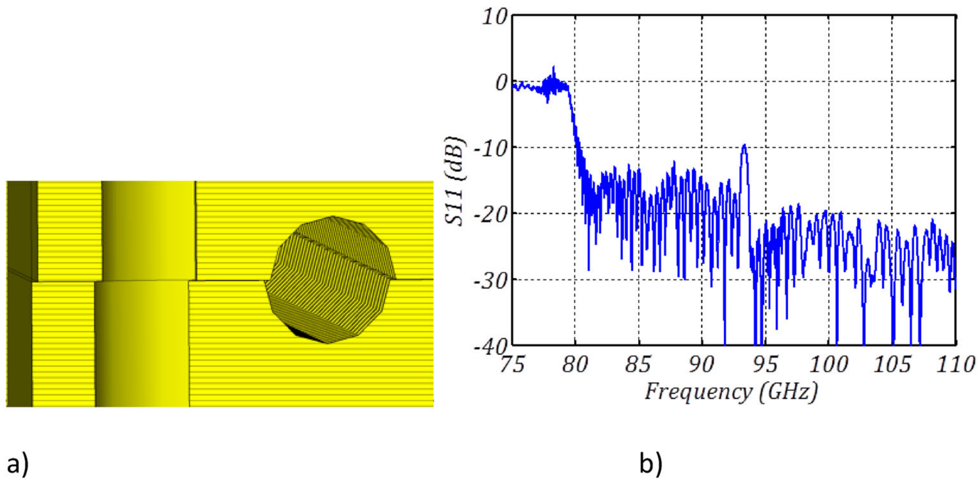


Figure 21. 94 GHz Folded waveguide: (a) misalignment model; (b) stop band due to misalignment [82].

Usually, an FWG is designed to work with beam voltage in the range of 10–20 kV. The Folded Waveguide is the most widely used among the SWSs at millimeter and sub-THz frequencies. This is due to the easy design, good coupling, wide band, and relatively high interaction impedance. However, the fabrication has to be done in two identical halves (both by LIGA or CNC milling) that are then bonded in a single block. The alignment of the two halves has to be highly accurate, otherwise the electromagnetic properties could be degraded. As an example (Figure 21), about 10 micron misalignment between the two halves (a) in a 92–95 GHz FWG generates a stop band at about 94 GHz (b), making the FWG not usable [82]. The improvement of the alignment accuracy permitted to remove the rejection band.

In the following, the most relevant FWG TWTs from 80 GHz to about 1 THz will be described, highlighting the variety of performance and approaches.

4.4.2. Folded waveguide TWTs below 100 GHz

Three FWG TWTs will be described below 100 GHz; some more were produced. A W-band (88–92 GHz) FWG TWT was presented in [97] with 38 dBm output power (Figure 22).

A modified FWG, the ridge-loaded FWG, built by CNC milling (Figure 23), was used for a W-band TWT that produced 25 W over the 93.1–94.8 GHz band [103]. It is notable that output powers up to 100 W are reported, considering that solid state GaN PA can provide a few Watts for the most advanced amplifiers.

A 91–101 GHz pulsed FWG TWTproduced 100 W output power with 6.7 GHz bandwidth and over 33 dB saturated gain at 20% duty cycle. The FWG was built by the LIGA process [114].

4.4.3. Folded waveguide TWTs in the range 100–220 GHz

The range above 100 GHz is gaining interest for wireless communications. A 140-GHz FWG TWT with an increased beam tunnel to improve the output power was reported in [115].

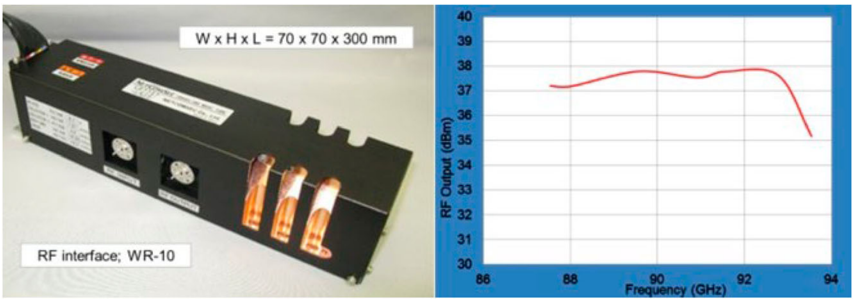


Figure 22. W-band TWT: (a) TWT, (b) Output power [97].

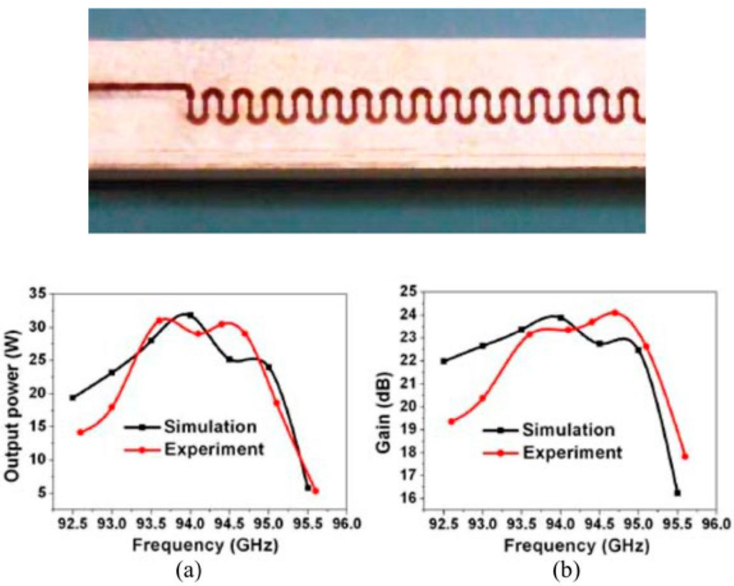


Figure 23. Ridge-loaded FWG, output power and gain [103].

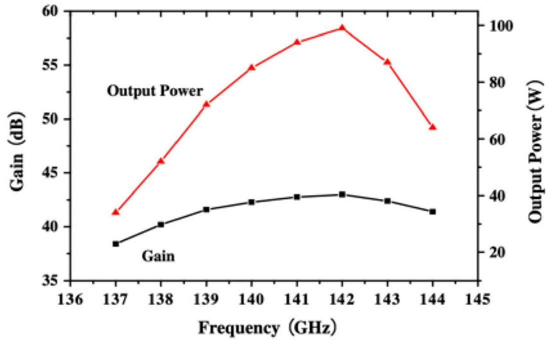


Figure 24. Simulated Gain and output power of 140 GHz FWG TWT with increased beam tunnel [115].

The TWT was designed to produce more than 80 W output power (Figure 24). The first experimental prototype provided output power of 1.6 W with a gain of 25 dB.

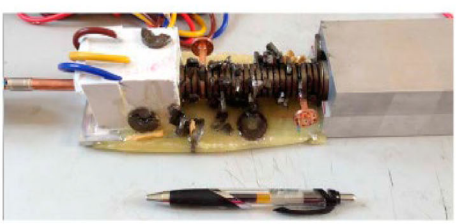
A D-band FWG TWT with 7.3W, 25.3 dB gain, and 3 GHz bandwidth at 140.3 GHz center frequency is reported in [116] (Figure 25). The short length of the interaction section is noteworthy. The FWG was built by CNC machining.

To increase the power, a 220 GHz TWT was based on a folded waveguide circuit array with five FWGs coupled together (Figure 26(a)) to achieve about 180 W. It required a multi-beam (5) cathode and high aspect-ratio planar permanent magnet (Figure 26(b)) [117].

The UV-LIGA process was used to manufacture the FWG for 220-GHz TWT with 0.2 W output power in the band 212–221 GHz at 0.1% duty cycle (Figure 27) [118].

A 220 GHz FWG TWT was presented in [119] with instantaneous 3 dB bandwidth of 8.8 GHz, and 350 mW peak power and about 16 dB gain (Figure 27). 15.7 kV beam voltage was used.

A different configuration of FWG TWT based on third harmonic amplification demonstrated 500 mW in the band 171.4–182.8 GHz (Figure 28). The harmonic amplification is obtained by two sections of FWG. The first section amplifies the input signal at 43.5–45.5 GHz that is then multiplied by three by a second FWG section at 130.5–136.5 GHz [120].



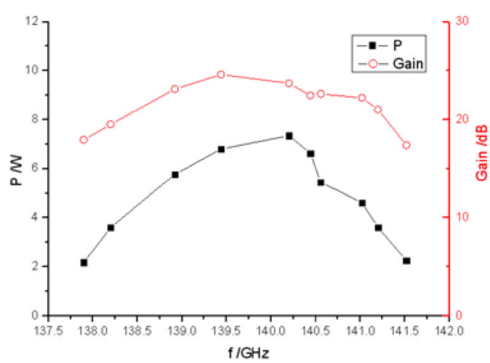


Figure 25. (a) Realized TWT, (b) Gain and output power [116].

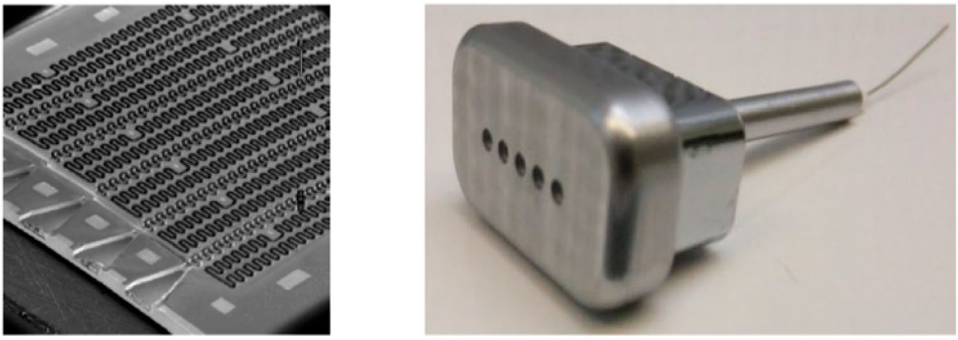


Figure 26. (a) 5-Folded waveguide circuit; (b) 5 beam cathode and [117].

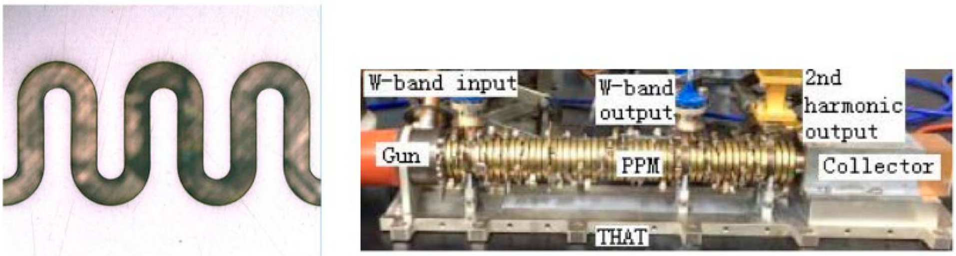


Figure 27. (a) LIGA FWG, (b) realized TWT [118].

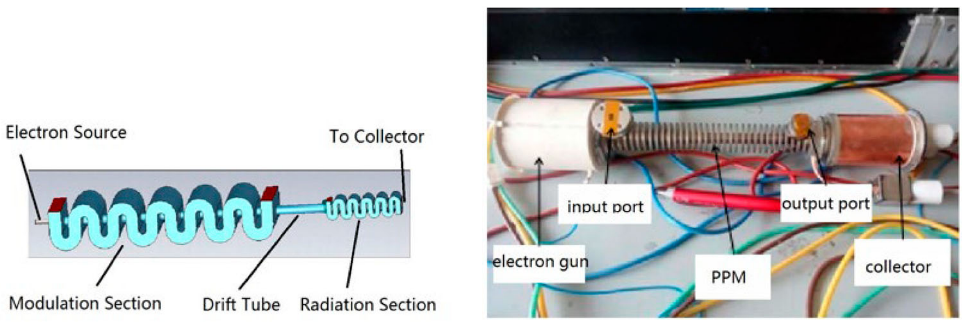


Figure 28. (a) FWG circuit with two sections at different frequency. (b) realized TWT, the input flange at Q-band and the output flange at D-band [120].

4.4.4. Folded waveguide TWT above 220 GHz

Above 220 GHz, the most advanced configurations of FWG TWT were reported touching the threshold of 1 THz [121–124]. The fabrication of the FWG, due to the very short wavelength (below 1.5 mm) is mostly performed by LIGA. Some samples were built by CNC milling utilizing nano CNC milling and tooling in the range of 100-micron diameter.

A FWG circuit realized by utilizing deep reactive ion etching (DRIE) and copper plating (Figure 29(a)) was used in a 233 GHz TWT (Figure 29(b)) demonstrating an output power greater than 50 W over a 2.4 GHz instantaneous bandwidth (Figure 29(c)) [122].

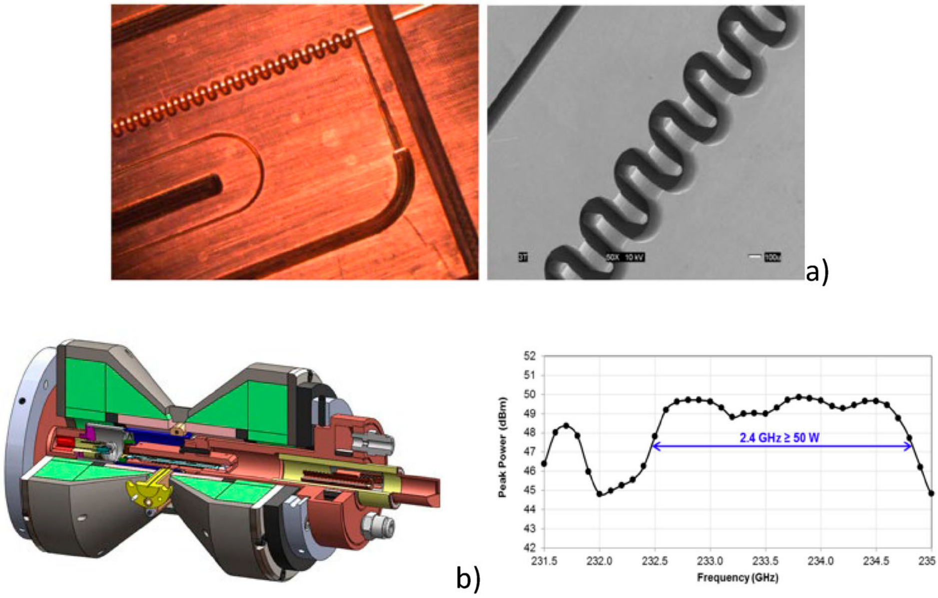


Figure 29. Details of the (a) FWG, (b) cross-section of the TWT and (c) output power as function of frequency [122].

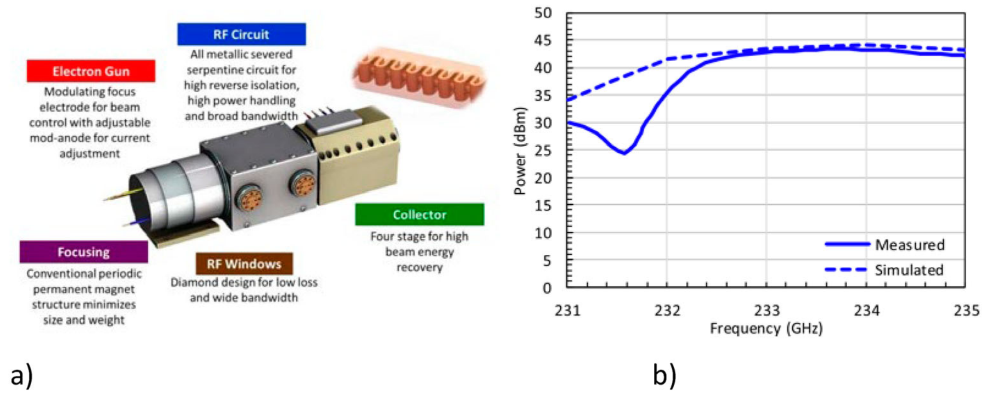


Figure 30. (a) G-band FWG TWT rendering and (b) measured output power [26].

Similar performance are reported for a 231.5–235 GHz FWG TWT (Figure 30(a)) providing a peak output power of 32 W (Figure 30(b)) [26]. The TWT was designed to be integrated into an (Microwave Power Module) MPM for VISAR applications [14].

A 320 GHz FWG TWT has been fabricated with an FWG realized by high speed high precision milling machining (details in Figure 31(a,b)). The TWT (Figure 31(c)) achieved 130 mW of maximum output power and 19.6 dB gain at 318.24 GHz (Figure 31(d)) [123].

A 0.670 THz Power Module based on an FWG TWT driven by a solid-state power amplifier (SSPA) has produced more than 100 mW with 21.5 dB gain in the 0.640–0.685 THz range in a bread-board demonstration. The TWT is based on a folded waveguide slow-wave circuit built by DRIE [124]. An 850 GHz FWG vacuum tube demonstrated 50 mW of output power in the band 0.835–0.842 THz and 39.4 mW at 0.850 THz [21].

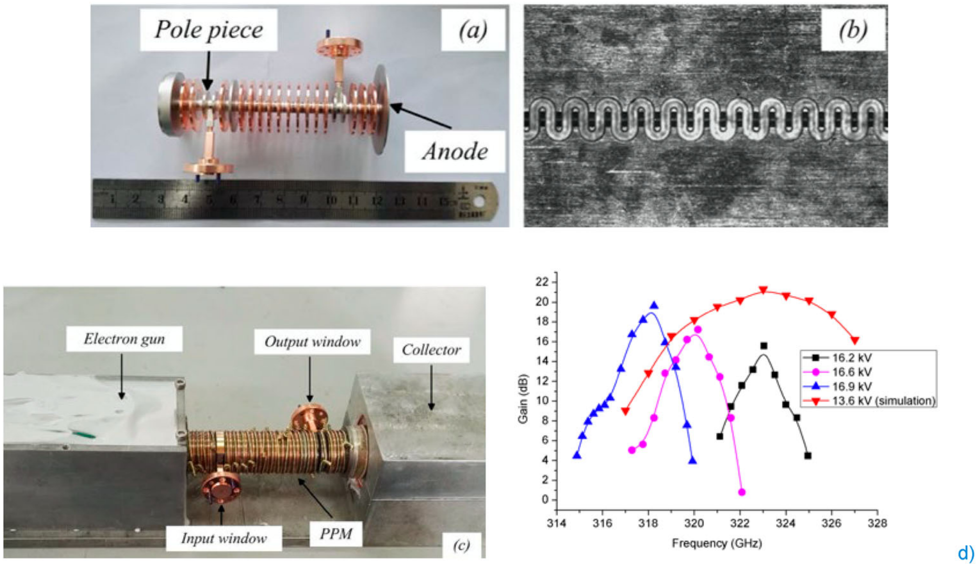


Figure 31. (a) Brazed high-frequency system including FWG, pole pieces, RF windows, and anode. (b) FWG half structure fabricated by the high-speed precision milling technology. (c) 0.32-THz FWG TWT [123].

The 1 THz FWG TWT reported in [19] is the highest frequency TWT measured. It was built by a high precision OFHC- copper electroplated folded waveguide (FWG) made by 2-level, deep reactive-ion etching (DRIE) of silicon-on-insulator (SOI) wafers (Figure 32(a)). The waveguide dimensions are in the order of tens of microns. The TWT (Figure 32(b)) demonstrated 29 mW power at 1.03 THz with 20 dB of saturated gain (Figure 32(c)).

The magnetic focusing of the last three FWG TWTs described was provided by permanent magnet solenoid.

Finally, the development of such a wide range of FWG TWTs demonstrates the FWG as a very flexible SWS. Most of the prototypes presented were a first trial; further improvements are expected in the future.

4.4.5. Double staggered waveguide

In early 2001, based on the previous analytic analysis of the rippled waveguide [125], the planar microfabricated sheet beam traveling-wave tube (TWT) amplifiers have been designed to satisfy the need for high-frequency, high-power sources of advanced radar and communication systems above 100 GHz, with peak powers of several hundred watts, and bandwidths of up to 10% [126]. As shown in the Figure 33, this structure consists of a rectangular waveguide including a rectangular grating leading to EM wave diffraction. This SWS supports a sheet beam permitting the use of a high beam current with a low beam current density, due to the wide cross section. The sheet beam can be focused by a periodically cusped magnetic system [127]. In order to improve the beam-wave interaction efficiency by increasing the coupling impedance, a planar ridge waveguide was investigated Figure 34(a) [126]. Further improvements were obtained by the double staggered grating (DSG) SWS, shown in Figure 34(b), in terms of ultra-wide operation frequency band [128–131].

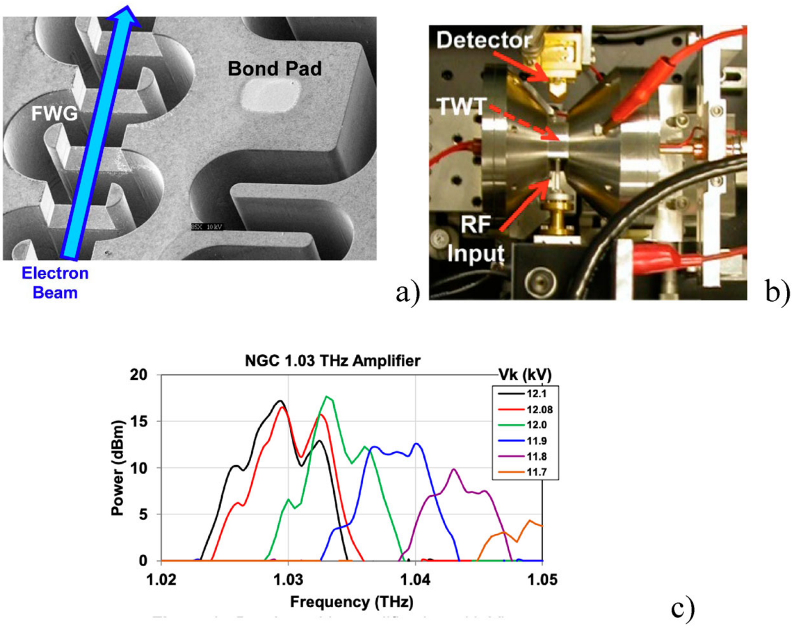


Figure 32. (a) SEM image of a FWG halve after Cu plating, prior to bonding, (b) 1.03 THz TWT [19], (c) output power measured at different beam voltage.

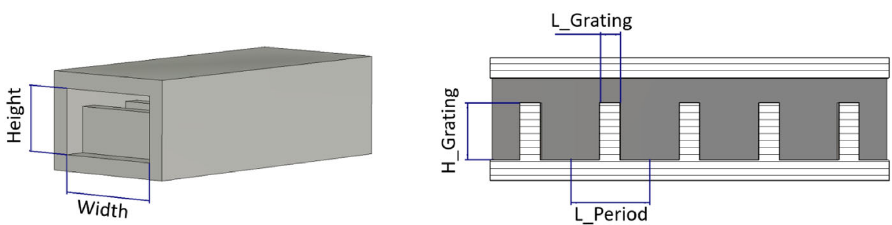


Figure 33. Planar Grating SWS [126].

The DSG can be fabricated both by CNC milling and LIGA. A DSG was fabricated by LIGA using KRPM photoresist to operate in the frequency range 214–266 GHz [85]. The RF measurements demonstrated excellent RF transmission with insertion loss fluctuating between 5 and 10 dB and the return loss fluctuating by + 3 dB around 7.5 dB [132]. To improve the electrical behavior, the Nano-CNC milling has been used to manufacture the DSG [79]. The cold test results showed 5 dB insertion loss and −10 dB return loss in the 200–265 GHz range. A 220-GHz Sheet Beam TWT amplifier, employing a Nano-CNC DSG circuit (Figure 35(a)), developed under the Defense Advanced Research Projects Agency (DARPA) HiFIVE program, provides more than 24 dB gain over the frequency range of 207–221 GHz, for 20.9 kV beam voltage (Figure 35(b)). In the high-gain operation mode, with 21.8 kV beam voltage, over 30 dB of gain was measured over the frequency range of 197–202 GHz [80].

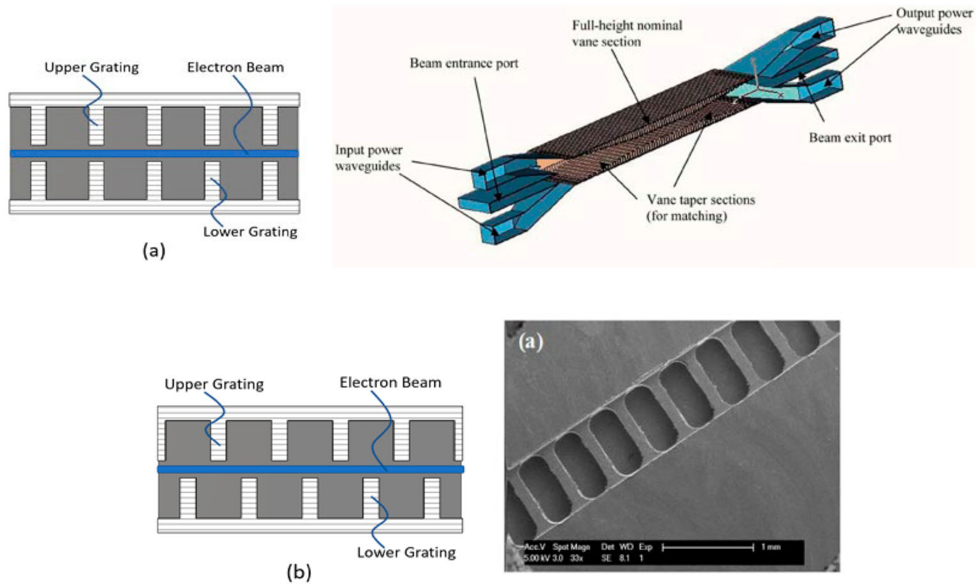


Figure 34. (a) Rectangular Grating Waveguide [125], (b) double staggered waveguide.

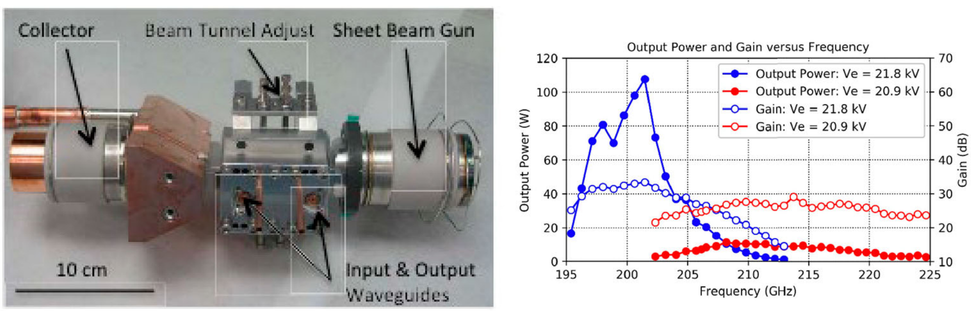
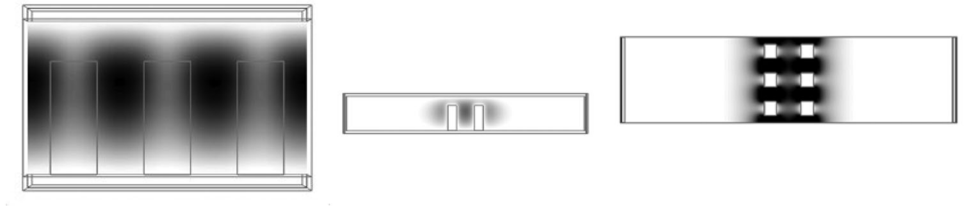


Figure 35. (a) 220 GHz DGS TWT, (b) output power [79].

4.4.6. Double corrugated waveguide

The double corrugated waveguide (DCW) was conceived for the first 1 THz backward wave tube realized in the frame of the OPTHER project [70]. The challenge of the project, due to the short wavelength, was to find an SWS able to support a cylindrical beam and feasible by micromachining. The only available solution was the structure used in the carcinotron [45], but its low interaction property allows very low gain and power.

The core of the DCW consists of two rows of parallel pillars in a rectangular waveguide. It was discovered that if two pillars are close to each other and have small cross-section, a quasi-round electric field is established between the two pillars (Figure 36). The space between the two rows is the beam channel. The beam axis position needs to be optimized depending on the DCW size and frequency. The mode propagating in the DCW is a hybrid TE_{10}. Of great importance is the design of the coupler to provide the best match with the TE_{10} mode at the flanges. The DCW demonstrated up to 2 Ω interaction impedance up to



a) b) c)

Figure 36. DCW Field distribution (a) side, (b) front, (c) top.

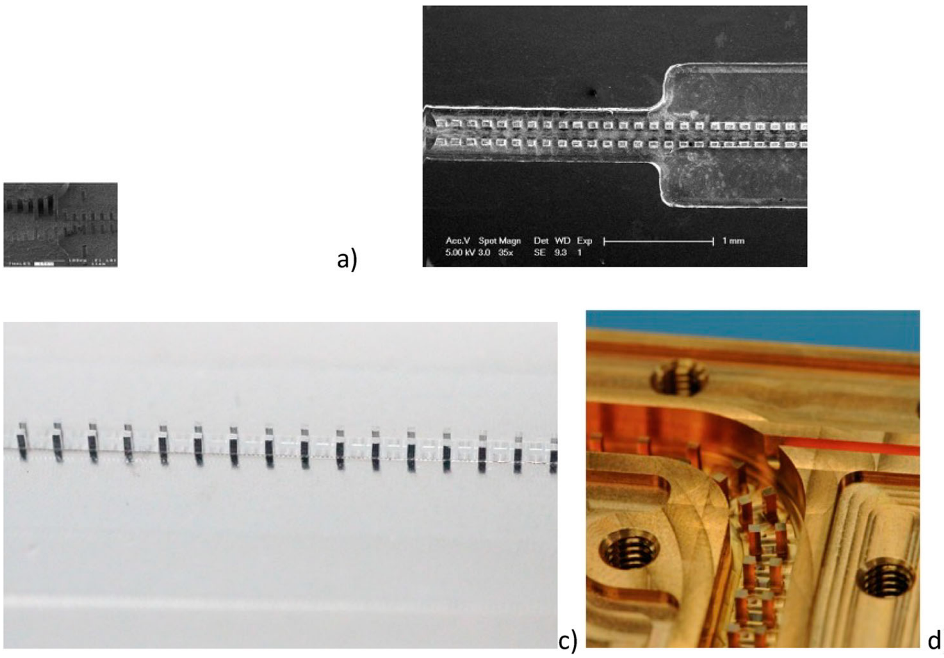


Figure 37. DCW at different frequencies (a) 1THz [70], (b) 0.346 THz [13], (c) 94 GHz, (d) 34 GHz [134].

1 THz. This value permits a good interaction beam-wave at that frequency. The fabrication of the DCW (pillar dimensions $20 \times 20 \times 60$ microns) was performed by deep-X-ray LIGA [70].

The DCW was built for many different frequency bands, from 30 GHz to 1 THz by different micromachining processes, such as CNC milling [134,135], and UV LIGA [73] (Figure 37). In all the cases, it has demonstrated very good dispersion and interaction impedance. The flexibility of the DCW permitted the use of different coupler topologies depending on the fabrication process (e.g. LIGA does not permit the tapering of the height of pillars). A Backward Wave Amplifier at 1 THz was built by using the first 1 THz DCW realized by deep-Xray LIGA [70] (Figure 38).

A number of projects are in progress to implement the DCW in traveling wave tubes and backward wave oscillators at millimeter waves [136,137].

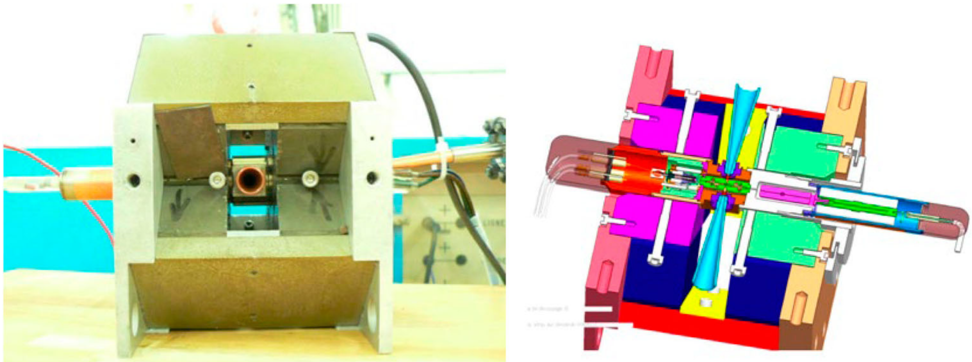


Figure 38. 1 THz Backward Wave Amplifier; (a) realization, (b) schematic [70].

5. Conclusions

TWTs, and in general vacuum electronics devices at millimeter waves, are in a phase of rapid evolution from the traditional microwave helix TWTs to innovative topologies, born to overcome the fabrication challenges that the short wavelength at millimeter wave poses. This review paper has covered the major advancements in the field, including new fabrication processes and topologies and provided the fundamental background to appreciate the technological steps and the state of the art of millimeter waves and THz TWT. The road for a commercialization and wide use of millimeter wave TWT starts to be defined. Applications in many fields, such as wireless communications, plasma diagnostics, security, non-destructive product inspection, healthcare, will benefit of their high output power over a wide bandwidth above 100 GHz, so far not available. The relevant progress of the last years and the huge effort worldwide will bring substantial progress in year to come, revolutionizing the oldest electronic device technology.

Acknowledgements

The work has received funding from the European Union's Horizon 2020 research and innovation programs under grant agreement no 762119, from EPSRC DLINK – D-band Wireless Link with Fibre Data Rate grant EP/S009620/1 in the UK, and from DOE DE-FG02-99ER54518 and DE-FG02-99ER54531 in the US.

Disclosure statement

No potential conflict of interest was reported by the authors.

Funding

This work was supported by Engineering and Physical Sciences Research Council [grant number EP/S009620/1]; Horizon 2020 Framework Programme [grant number 762119]; DOE [grant number DE-FG02-99ER54518,DE-FG02-99ER54531].

Notes on contributors

Claudio Paoloni, since 2012, has been Cockcroft Chair with the Engineering Department, Lancaster University, U.K. Since 2015, he has been the Head of Engineering Department. He is member at large of

the Board of Governor of the IEEE Electron Devices Society and Chair of the IEEE EDS Vacuum Electronics Technical Committee (2017 - present). He is Senior Fellow of the Higher Education Academy. He was Guest Editor for the 2014 Special Issue of Transaction on Electron Devices on V acuum Electronics. He is coordinator of two European Commission Horizon 2020 projects, TWEETHER and ULTRAWAVE. He is author of more than 230 articles in journals and international conferences in the field of sub-THz vacuum electronic devices and wireless communications.

Dr Diana Gamzina joined SLAC in January of 2017; she was at the UC Davis millimeter-wave research group for over 8 years prior to that leading research and development programs in millimeter wave and terahertz vacuum electronics. At SLAC, she has focused on development of advanced materials for vacuum electron devices. Her expertise includes mechanics of materials' interaction with electromagnetic waves, micro to nano scale as well as additive material synthesis techniques, high current density nano-composite cathodes, and multiscale thermo-mechanical design and analysis. Enabling design driven material microstructure for the next generation of RF vacuum electronic devices is her personal career goal.

Rosa Letizia received the Laurea degree in Electronic Engineering from the Polytechnic of Bari, Bari, Italy, and the Ph.D. degree in computational photonics from the University of Leeds, Leeds, U.K., in 2005 and 2009, respectively. In 2011, she joined the Engineering Department, Lancaster University, Lancaster, U.K., and the Cockcroft Institute of Accelerator Science and Technology, Warrington, U.K., where she has been a Senior Lecturer since 2019. In 2019, she was the recipient of the Senior Research Fellowship from The Leverhulme Trust and Royal Academy of Engineering. She is an IEEE Senior Member and serves as an associate editor for the IEEE Transactions on Electron Devices.

Yuan Zheng received the B.S. (2010), and Ph. D. (2016) degree in vacuum electronics from the University of Electronic Science and Technology of China, Chengdu, China. After graduation, he joined the Davis MM-wave Research Center in 2016 as a Post-Doc scholar. He is now a project scientist in UC Davis mm-Wave Research Group focusing on sheet beam high-power millimeter-wave devices, including SB-TWTs, SB-BWOs and SB-klystrons.

Neville C. Luhmann Jr. was awarded the Ph.D. in Physics at University of Maryland, College Park, (1972). He is Professor, Electrical and Computer Engineering Department, University of California, Davis (1993-Present). He was Professor, Department of Applied Science, University of California, Davis (1993 – 2011) and Professor at Department of Electrical Engineering, University of California, Los Angeles (1981–1993). He has published approximately 392 papers in archival journals, 375 proceedings articles, and 18 books and chapters, and 1086 conference presentations. He is Fellow of the American Physical Society, Fellow of the Institute of Electrical and Electronic Engineering, Recipient of the IEEE Plasma Science and Applications Committee (PSAC) Award for Outstanding Contributions to the Field of Plasma Science, He was awarded the Kenneth J. Button Award for "Recognition of Outstanding Contributions to the Science of the Electromagnetic Spectrum" 2005. This is administered by The Institute of Physics (London). He is UC Davis Distinguished Professor.

ORCID

Claudio Paoloni http://orcid.org/0000-0002-0265-0862
Rosa Letizia http://orcid.org/0000-0002-1664-2265
Yuan Zheng http://orcid.org/0000-0001-9674-1353

References

[1] Gewartowski JW, Watson HA. *Principles of electron tubes*. Princeton, NJ: Van Nostrand; 1965.
[2] Whitaker J. *Power vacuum tubes handbook*. CRC Press; 1999.
[3] Barker RJ, et al. *Modern microwave and millimeter-wave power electronics*. Wiley-IEEE Press; 2005.
[4] Gilmour AS. Klystrons, Traveling wave tubes, magnetrons, crossed-field amplifiers, and gyrotrons. Artech House Microwave Library, 2011.

[5] Carter R. *Microwave and RF vacuum electronic power*. Cambridge University Press; 2018.
[6] Shulim T. Electron beams and microwave vacuum electronics. 512 P. Hoboken, NJ: John Wiley & Sons, Inc.; November 2006.
[7] Minenna D, André F, Elskens Y, et al. The traveling-wave tube in the history of telecommunication. Euro Phys J H. 2019;44(1):1–36.
[8] Kompfner R. The traveling wave valve. Wireless World. 1946;52(11):369–372.
[9] Kompfner R. The traveling-wave tube as amplifier at microwaves. Proc IRE. 1947;35(2):124–127.
[10] Kompfner R. *The invention of the traveling-wave tube*. San Francisco Press; 1964.
[11] Federici JF, Schulkin B, Huang F, et al. THz imaging and sensing for security applications—explosives, weapons and drugs. Semicond Sci Technol. 2005;20(7):S266–S280.
[12] Li X, Huang X, Mathisen S, et al. Design of 71-76 GHz double-corrugated waveguide traveling-wave tube for satellite downlink. IEEE Trans Electron Devices. 2018;65(6):2195–2200.
[13] Feng J, Tang Y, Gamzina D, et al. Fabrication of 0.346 THz BWO for Plasma Diagnostics. IEEE Transactions on Electron Devices, 8 p. March 2018.
[14] Kim R, Dominski F. ViSAR: a 235 GHz radar for airborne applications. 2018 IEEE Radar Conference (RadarConf18), Oklahoma City, OK, 2018, pp. 1549–1554.
[15] Field M, Kimura T, Atkinson J, et al. Development of a 100-W 200-GHz high bandwidth mm-wave amplifier. IEEE Trans Electron Devices. 2018;65(6):2122–2128. DOI:10.1109/TED.2018.2790411
[16] Baig A, et al. 0.22 THz wideband sheet electron beam traveling wave tube amplifier: cold test measurements and beam wave interaction analysis. Phys Plasmas. 2012;19(093110.
[17] Baig A, et al. Design, fabrication and RF testing of near-THz sheet beam TWTA. Terahertz Sci Technol. 2011;4.
[18] Paoloni C, Mineo M. 0.22 THz TWT based on the double corrugated waveguide. IEEE International Vacuum Electronics Conference, 22–24 April 2014.
[19] Tucek JC, et al. Operation of a compact 1.03 THz power amplifier. IEEE International Vacuum Electronics Conference, 2016.
[20] Tucek JC, et al. 0.850 THz vacuum electronic power amplifier. IEEE International Vacuum Electronics Conference, 2014.
[21] Basten MA, et al. 0.850 THz Vacuum Electronic Power Amplifier. Vacuum Electronics Conference (IVEC), 2012 IEEE Thirteenth International, 2012.
[22] Paik SF. Design formulas for helix dispersion shaping. IEEE Trans Electron Devices. 1969; 16(12).
[23] Zhu ZJ, Wei CL. Simulation modeling on dispersion shaping and harmonic suppression In helix Twt from 2 GHz to 6 GHz. Prog Electromagn Res C. 2012;28:181–193.
[24] Gittins JF. *Power Travelling-wave tubes*. New York: American Elsevier Publishing Company; 1965.
[25] Smith CR, Armstrong CM, Duthie J. The microwave power module: a versatile RF building block for high-power transmitters. Proc IEEE. 1999;87(5):717–737.
[26] Armstrong CM, Kowalczyk R, Zubyk A, et al. A compact extremely high frequency MPM power amplifier. IEEE Trans Electron Devices. 2018;65(6):2183–2188. DOI:10.1109/TED.2018.2808327
[27] Springmann D, Chan D, Schoemehl T, et al. A 50W Ka-band NanoMPM®. IEEE International Vacuum Electronics Conference, Monterey, CA, 2014, pp. 123–124. doi:10.1109/IVEC.2014.6857520.
[28] Marchewka C, et al. Recent Results on a 26 40 GHz Ka-band MPM. 2007 IEEE International Vacuum Electronics Conference, Kitakyushu, 2007, pp. 1–2. doi:10.1109/IVELEC.2007.4283235.
[29] Taylor J, Chan D, Donald A, et al. An 80 Watt dual Ka/Q-band mini-TWT. 2013 IEEE 14th International Vacuum Electronics Conference (IVEC), Paris, 2013, pp. 1–2, doi:10.1109/IVEC.2013.6571094.
[30] Kowalczyk R, et al. High efficiency E-band MPM for communications applications. 2016 IEEE International Vacuum Electronics Conference (IVEC), Monterey, CA, 2016, pp. 1–2, doi:10.1109
[31] Wan C, et al. "A 100 Watt W-Band MPM," 2013 IEEE 14th International Vacuum Electronics Conference (IVEC), Paris, 2013, pp. 1–1, doi:10.1109/IVEC.2013.6571011.
[32] Chen J, Wang F, Zhang Z, et al. A 50 Watt W-band MPM, 2020 IEEE International Vacuum Electronics Conference (IVEC), virtual.
[33] Jung AR. 10 kW and Up, from a Helix TWT? Proc. of International Electron Devices Meeting, 1978.
[34] Hobrecht CE. Resonant loss for helix traveling wave tubes. Proc. of International Electron Devices Meeting, 1977.

[35] Chong CK, Davis JA, LeBorgne RH, et al. Development of high-power Ka-band and Q-band helix-TWTs. IEEE Trans. Electron Devices. 2005;52(5):653–659.
[36] Chong CK, Forster JW, Layman DA, et al. Ka-band satellite uplink high-power helix TWTs: output power evolution at L-3 ETI, International Electron Devices Conference, May 2010, pp. 53–54.
[37] Chong CK, Layman DA, Stolz RJ, et al. Development of high-power K/Ka-band helix TWT. International Electron Devices Conference, April 2012, pp. 119–120.
[38] LeBorgne RH, et al. Development of an 800W Ka-Band, Ring-Bar TWT. International Technical Digest on Electron Devices Conference 1990, Dec. 1990.
[39] Wilson D. A millimeter-wave tunneladder TWT final report, NASA Contract Report 182183, Oct. 1988.
[40] Kosmahl HG, Palmer RW. Harmonic analysis approach to the "tunneladder": a modified Karp circuit for millimeter-wave TWTA's. IEEE Trans Electron Devices. 1982;29(5):862–869.
[41] Karp A. Traveling wave tube experiments at millimeter wavelength with a new, easily built, space harmonic circuit. Proc IRE. 1955;43:41–46.
[42] Karp A. *Millimeter wave valves, Fortschritte der Hochfrequenztechnik*, Vol. 5. Frankfurt/Main: Academlc Press MBH; 1960, pp. 73–128.
[43] Craig RA, Hiramatsu Y. A pulsed 10 megawatt travelling-wave tube amplifier. Proceedings of the International Congress on Microwave Tubes, Munich, Germany, pp.94–97, 1960.
[44] Chodorow M, Pearce AF, Winslow DK. The centipede high power traveling wave tube. Microwave laboratory, report no. 695 Stanford University, 1960.
[45] Chalk GO, Chalmers PM. A 500 KW travelling wave tube for x-band. 6th Int. Conf. on Microwave and Optical Generation and Amplification, Cambridge, England, pp. 54–58, 1966.
[46] Roumbanis T, Needle J, Winslow DK. A megawatt x-band TWT amplifier with 18% bandwidth. Proc. of the High-Power Microwave Symposium, 1 The Hexagon, Fort Monmouth, New Jersey, pp. 114–129, 1962.
[47] Heffner H. Analysis of the backward-wave traveling-wave tube. Proc IRE, pp. 930–937. June 1954.
[48] Johnson HR. Backward-wave oscillators. Proc. of IRE, pp. 684–697, June 1955.
[49] Grow RW, Watkins DA. Backward wave oscillator efficiency. Proc IRE, pp. 848–856, July 1955.
[50] Karp A. Backward-wave oscillator experiments at 100 to 200 kilomegacycles. Proc. of the I.R.E. 1957;45:496–503.
[51] Palluel P, Goldberger AK. The 0-type carcinotron tube. Proc. of the I.R.E, pp. 333–345. March 1956.
[52] Kantorowicz G, Palluel P, Oscillators BW. *Infrared and millimeter waves* by K.J. Button. New York: Academic Press; 1979.
[53] Forster DC. High power millimeter wave sources. Adv Microwaves. 3;1968:301–346.
[54] Lewen F, et al. Phase locked backward wave oscillator pulsed beam spectrometer in the submillimeter wave range. Rev Sci Instruments. 1998;69(32).
[55] van Ardenne A, Woestenburg EEM, van der Ree LJ. 350-GHz phase/frequency locked loop for use with a carcinotron backward wave oscillator. Rev Sci Instruments. 1986;57:2547–2553.
[56] van Vliet AHF, et al. A low noise heterodyne receiver for astronomical observations operating around 0.63 mm wavelength. Int J Infrared Millimeter Waves. 1982;3(6).
[57] Keen NJ, et al. Low-noise 460 GHz waveguide Schottky mixer radiometer for radioastronomy. Electron Lett. 1986;22(7): 353–355.
[58] Luhmann Jr NC, et al. Millimeter and submillimeter wave diagnostic systems for contemporary fusion experiments. In: DKPE Stott, G Gorini, E Sindoni, editors. *Diagnostics for Contemporary fusion Experiments*. Bologna: SIF; 1991. p. 135–117.
[59] Hartfuß HJ, Geist T. Fusion plasma diagnostics with Mm waves. Weinheim (Germany): Wiley-VCH Verlag GmbH & Co. KGaA; 2013; [Online]. Available from: http://www.wiley-vch.de
[60] Hartfuss HJ. RF techniques in plasma diagnostics. Plasma Phys Controlled Fusion. 1998;40(8A): A231–A250.
[61] Hartfuss HJ, Geist T, Hirsch M. Heterodyne methods in millimetre wave plasma diagnostics with applications to ECE, interferometry and reflectometry. Plasma Phys Controlled Fusion. 1997;39(11):1693–1769.

[62] Luhmann, Jr. NC, Bindslev H, Park H, et al. Microwave diagnostics. Fusion Sci Technol. 2008;53(2):335–396.
[63] Luhmann, Jr. NC, Peebles WA. Instrumentation for magnetically confined fusion plasma diagnostics. Rev Sci Instruments. 1984;55(279).
[64] Kozlov G, Volkov A. Coherent source submillimeter wave, spectroscopy. In: Millimeter and submillimeter wave spectroscopy of solids. *Topics in applied physics*. vol. 74. Springer, 1998.
[65] Guidee P, Teyssier L. A 850 - 1000 GHz backward-wave oscillator for advanced applications. Proc. SPIE 0598, Instrumentation for Submillimeter Spectroscopy, April 1986.
[66] Teyssier L, Gerber R, Wideband A. High-power 0-type carcinotron operating near 94 GHz. Proc. of IEDM, Washington, 1987.
[67] Borisov AA, et al. The development of vacuum microwave devices in Istok. 2011 IEEE International Vacuum Electronics Conference (IVEC), 2011.
[68] Ives RL. Microfabrication of high-frequency vacuum electron devices. IEEE Trans Plasma Sci. 2004;32(3):1277–1291.
[69] Genolet G, Lorenz H. UV-LIGA: from development to commercialization. Micromachines (Basel). 2014;5:486–495.
[70] Paoloni C, Di Carlo A, Bouamrane F, et al. Design and realization aspects of 1-THz cascade backward wave amplifier based on double corrugated waveguide. IEEE Trans Electron Devices. 2013;60(3):1236–1243.
[71] Tucek C, et al. Operation of a compact 1.03 THz power amplifier. Vacuum Electronics Conference (IVEC), 2016 IEEE Thirteenth International, 2016.
[72] Makarova OV, Divan R, Tucek J, et al. Fabrication of solid copper two-level waveguide circuits for a THz radar system by UV lithography. 2016 IEEE International Vacuum Electronics Conference (IVEC), Monterey, CA, 2016, pp. 1–2.
[73] Malek Abadi SA, Paoloni C. UV-LIGA microfabrication process for sub-terahertz waveguides utilizing multiple layered SU-8 photoresist. J Micromech Microeng. 2016;26:095010.
[74] Joye CD, et al. Microfabrication of wideband distributed beam amplifiers at 220 GHz. In Vacuum Electronics Conference (IVEC), 2011 IEEE International, pp. 343–344, 2011.
[75] Joye CD, Calame JP, Nguyen KT, et al. Microfabrication of fine electron beam tunnels using UV-LIGA and embedded polymer monofilaments for vacuum electron devices. J Micromech Microeng. 2012;22:015010.
[76] Joye CD, et al. UV-LIGA and DRIE grating microfabrication and testing for sheet beam amplifiers at 220 GHz. In Infrared Millimeter and Terahertz Waves (IRMMW-THz), 2010 35th International Conference on, 2010, pp. 1–2.
[77] Joye CD. UV-LIGA Microfabrication of 220 GHz sheet beam amplifier gratings with SU-8 photoresists. J Micromechan Microeng. 2010;20:125016.
[78] Joye CD, Kimura T, Hyttinen M, et al. Demonstration of a high power, wideband 220-GHz traveling wave amplifier fabricated by UV-LIGA. IEEE Trans Electron Devices. 2014;61(6):1672–1678.
[79] Barchfeld R A G, et al. Microfabrication of terahertz vacuum electronics devices. American Society for Precision Engineers Conference, 2011.
[80] Baig A, Gamzina D, Kimura T, et al. Performance of a nano-CNC machined 220-GHz traveling wave tube amplifier. IEEE Trans Electron Devices. 2017;64(5):2390–2397.
[81] Gamzina D, Himes LG, Barchfeld R, et al. Nano-CNC machining of sub-THz vacuum elec-tron devices. IEEE Trans Electron Devices. 2016;63(10):4067–4073. DOI:10.1109/TED.2016.2594027
[82] André F, Racamier J-C, Zimmermann R, et al. Technology, assembly, and test of a W-band traveling wave tube for new 5G high-capacity networks. IEEE Trans Electron Devices. 2020;67(7):2919–2924. DOI:10.1109/TED.2020.2993243
[83] Paoloni C, Krozer V, Magne F, et al. D-band point to multi-point deployment with G-band transport. European Conference on Networks and Communications 2020.
[84] Elmer JW, Klingmann J, Van Bibber K. Diffusion bonding and brazing of high purity copper for linear collider accelerator structures. Phys Rev ST Accel Beams. 2001;4:053502.
[85] Carlsten BE, et al. Stability of an emittance-dominated sheet-electron beam in planar wiggler and periodic permanent magnet structures with natural focusing. Phys Rev ST Accel Beams. 2005;8(062001):1–14.

[86] Booske JH, McVey BD, Antonsen Jr. TM. Stability and confinement of nonrelativistic sheet electron beams with periodic cusped magnetic focusing. J Appl Phys. 1993;73(9):4140–4155.
[87] Booske JH, Basten MA, Kumbasar AH, et al. Periodic magnetic focusing of sheet electron beams. Phys Plasmas. 1994;1(5):1714–1720.
[88] Field M, Kimura T, Atkinson J, et al. Development of a 100-W 200-GHz high bandwidth mm-wave amplifier. IEEE Trans Electron Devices. 2018;65(6):2122–2128. DOI:10.1109/TED.2018.2790411
[89] Wang J-X, et al. Electron beam transport analysis of W-band sheet beam klystron. Phys Plasmas. 2010;17:043111.
[90] Zheng Y, Gamzina D, Himes L, et al. Design and analysis of the staggered double grating slow wave circuit for 263 GHz sheet beam TWT. IEEE Trans Terahertz Sci Technol. 2020;10(4):411–418. DOI:10.1109/TTHZ.2020.2995826
[91] Shen F, Wei Y, Yin H, et al. A novel V-shaped microstrip meander-line slow-wave structure for W- band MMPM. IEEE Trans Plasma Sci 2012;40(2):463–469. DOI:10.1109/tps.2011.2175252
[92] Shen F, Wei Y, Xu X, et al. Symmetric double V-shaped microstrip meander- line slow-wave structure for W-band traveling-wave tube. IEEE Trans Electron Devices. 2012;59(5):1551–1557. DOI:10.1109/Ted.2012.2188635
[93] Li X, et al. Study on phase velocity tapered microstrip angular log- periodic meander line travelling wave tube. IET Microw Antennas Propag. 2016;10:902–907. DOI:10.1049/iet-map.2015.0520
[94] Wang S, Hou Y, Wei Y, et al. Study on 800 V traveling-wave tube. High Power Laser Particle Beams. 2013;25(7):1613–1614. DOI:10.3788/HPLPB20132507.1613
[95] Wang S, Gong Y, Hou Y, et al. Study of a log-periodic slow wave structure for Ka-band radial sheet beam traveling wave tube. IEEE Trans Plasma Sci. 2013;41(8):2277–2282. DOI:10.1109/TPS.2013.2271639
[96] Wang S, Gong Y, Wang Z, et al. Study of the symmetrical microstrip angular log-periodic meander-line traveling- wave tube. IEEE Trans Plasma Sci. 2016;44(9):1787–1793. DOI:10.1109/TPS.2016.2598614
[97] Wang H, et al. Study of a miniaturized dual-beam TWT with planar dielectric-rods-support uniform metallic meander line. Phys Plasmas. 2018;25:Art. no. 063113. DOI:10.1063/1. 5023776
[98] Li X, Wang Z, He T, et al. Study on radial sheet beam electron optical system for miniature low-voltage traveling-wave tube. IEEE Trans Electron Devices. 2017;64(8):3405–3412. DOI:10.1109/TED.2017.2711616
[99] Zhao C, Aditya S, Chua C. Analysis of coupled planar helices with straight-edge connections for application in millimeter-wave TWTs. IEEE Trans Electron Devices. 2013;60(3):1244–1250. DOI:10.1109/TED.2013.2241437
[100] Nguyen KT, Cooke SJ, Levush B, et al. Design methodology and experimental verification of serpentine/folded-waveguide TWTs. IEEE Trans Electron Devices. 2014;61(6):1679–1686. DOI:10.1109/TED.2014.2303711
[101] Zhang X, Feng J, Cai J, et al. Design and experimental study of 250-W W-band pulsed TWT With 8-GHz bandwidth. IEEE Trans Electron Devices. 2017;64(12):5151–5156.
[102] Yoshida M, et al. Development activity of Terahertz amplifiers with FWG-TWTs. 2016 IEEE International Vacuum Electronics Conference (IVEC), Monterey, CA, 2016.
[103] Wei Y, Guo G, Gong Y, et al. Novel W-band ridge-loaded folded waveguide traveling wave tube. IEEE Electron Device Letters 2014;35(10):1058–1060.
[104] Hou Y, Gong Y, Xu J, et al. A novel ridge-vane-loaded folded-waveguide slow wave structure for 0.22-THz traveling-wave tube. IEEE Trans Electron Devices. 2013;60(3):1228–1235.
[105] Hou Y, Xu J, Yin H-R, et al. Equivalent circuit analysis of ridge-loaded folded- waveguide slow-wave structures for millimeter-wave traveling-wave tubes. Prog Electromagn Res. 2012;129:215–229. DOI:10.2528/PIER12042602
[106] Gong H, Gong Y, Tang T, et al. Experimental investigation of a high-power Ka-band folded waveguide traveling-wave tube. IEEE Trans Electron Devices. 2011;58(7):2159–2163. IEEE Transactions On Plasma Science, Vol. 47, No. 5, May 2019. DOI:10.1109/TED.2011.214 8119

[107] Gong H, et al. A high efficiency Q-band folded waveguide traveling- wave tube. Proc. IEEE Int. Vac. Electron. Conf., Monterey, CA, Apr. 2014, pp. 127–128. DOI:10.1109/IVEC.2014.6857522
[108] Liao M, et al. A V-band folded waveguide TWT. Proc. IEEE Int. Vac. Electron. Conf., Beijing, China, Apr. 2015, pp. 1–2. DOI:10.1109/IVEC.2015.7223937
[109] Zhang L, Wei Y, Guo G, et al. A ridge-loaded sine waveguide for G-band traveling- wave tube. IEEE Trans Plasma Sci. 2016;44(11):2832–2837. DOI:10.1109/Tps.2016.2605161
[110] Xu X, Wei Y, Shen F, et al. Sine waveguide for 0.22-THz traveling-wave tube. IEEE Electron Device Lett. 2011;32(8):1152–1154. DOI:10.1109/led.2011.2158060
[111] Fang S, et al. Study on W-band sheet-beam traveling-wave tube based on flat-roofed sine waveguide. AIP Adv. 2018;8:Art. no. 055116. DOI:10.1063/1.5028300
[112] Lei X, et al. Full-wave analysis of the high frequency characteristics of the sine waveguide slow-wave structure. AIP Adv. 2017;7:Art. no. 085111. DOI:10.1063/1.4997329
[113] Lei X, Li Q, Wu G, et al. Linear analysis of traveling sheet electron beam in sine waveguide tubes. J Appl Phys. 2018;124:Art. no. 133301. DOI:10.1063/1.5025373
[114] Feng J, Cai J, Hu Y, et al. Development of W-band folded waveguide pulsed TWTs. IEEE Trans Electron Devices. 2014;61(6):1721–1725.
[115] Wang Z, Zhou Q, Gong H, et al. Development of a 140-GHz folded-waveguide traveling wave tube in a relatively larger circular electron beam tunnel. J Electromagn Waves Appl. 2017;31(17):1914–1923.
[116] Wenqiang L, Yi J, Quanfeng Z, et al. Development of D-band continuous-wave folded waveguide traveling-wave tube. IEEE International Vacuum Electronics Conference (IVEC), 2015.
[117] Tucek JC, et al. 220 GHz power amplifier development at Northrop Grumman. Vacuum Electronics Conference (IVEC), 2012 IEEE Thirteenth International, pp. 553–554, 2012.
[118] Li H, Cai J, Du Y, et al. UV-LIGA microfabrication for high frequency structures of a Y-band TWT 2nd harmonic amplifier. Proc. IEEE Int. Vac. Electron. Conf. (IVEC), Apr. 2015, pp. 1–2.
[119] Zhou Q, et al. Development of a 0.22THz folded waveguide travelling wave tube. In: 2015 IEEE International Vacuum Electronics Conference (IVEC), Beijing, 2015, pp. 1-2. DOI:10.1109/IVEC.2015.7223971
[120] Gong HR, Wang Q, Deng D, et al. Third-harmonic traveling-wave tube multiplier- amplifier. IEEE Trans Electron Devices. 2018;65(6):2189–2194. DOI:10.1109/Ted.2017.2785661
[121] Pan P, et al. Development of 220 and 340 GHz TWTs. Proc. IEEE 9th UK-Eur.-China Workshop Millimetre Waves THz. Tech- nol. (UCMMT), Qingdao, China, Sep. 2016, pp. 39–41. DOI:10.1109/UCMMT.2016.7873954
[122] Basten MA, Tucek JC, Gallagher DA, et al. 233 GHz high Power amplifier development at Northrop Grumman. Proc. IEEE Int. Vacuum Electron. Conf. (IVEC), Apr. 2016, pp. 1–2.
[123] Hu P, Lei W, Jiang Y, et al. Development of a 0.32-THz folded waveguide traveling wave tube. IEEE Trans Electron Devices. 2018;65(6):2164–2169. DOI:10.1109/TED.2017.2787682
[124] Tucek JC, et al. A 100 mW, 0.670 THz power module. Vacuum Electronics Conference (IVEC), 2012 IEEE Thirteenth International, pp. 553–554, 2012.
[125] Carlsten BE, et al. Pierce gain analysis for a sheet beam in a rippled waveguide traveling wave tube. Phys Plasmas. 2001;8:4585–4591.
[126] Carlsten BE, Russell SJ, Earley LM, et al. Technology development for a mm-wave sheet-beam traveling-wave tube. IEEE Trans Plasma Sci. 2005;33(1):85–93.
[127] Basten MA, Booske JH. Two-plane focusing of high space charge sheet electron beams using periodically cusped magnetic fields. J Appl Phys. 1999;85(9):6313–6322.
[128] Shin YM, Barnett LR. Intense wideband terahertz amplification using phase shifted periodic electron-plasmon coupling. Appl Phys Lett. 2008;92(9):091501-1–091501-3.
[129] Available from: https://patents.google.com/patent/US7952287B2/en
[130] Zhang Y, Wang Z, Zhou Q, et al. A high-power single rectangular grating sheet electron beam traveling-wave tube. IEEE Trans Electron Devices. 2016;63(8):3262–3269. DOI:10.1109/ted.2016.2576464
[131] Shi X, Wang Z, Tang T, et al. Theoretical and experimental research on a novel small tunable PCM system in staggered double vane TWT. IEEE Trans Electron Devices. 2015;62(12):4258–4264. DOI:10.1109/Ted.2015.2483538

[132] Baig A, Gamzina D, Johnson M, et al. Experimental characterization of LIGA fabricated 0.22 THz TWT circuits. IEEE Int Vacuum Electron Conference (IVEC). 2011:275–276.
[133] Mineo M, Paoloni C. Double corrugation rectangular waveguide slow-wave structure for THz vacuum devices. IEEE Trans Electron Devices. 2010;57(11):3169–3175.
[134] Paoloni C, Mineo M, Henry M, et al. Double corrugated waveguide for Ka-band traveling wave tube. IEEE Trans Electron Devices. 2015;62:3851–3856.
[135] Paoloni C, Krozer V, Magne F, et al. D-band point to multi-point deployment with G-Band transport. at European Conference on Networks and Communications 2020.
[136] Basu R, Billa LR, Letizia R, et al. Design of sub-THz traveling wave tubes for high data rate long range wireless links. Semicond Sci. Technol. 2018;33:124009.
[137] Basu R, Billa LR, Letizia R, et al. Design of D-band double corrugated waveguide TWT for wireless communications. Proc. IEEE 20th Int. Vac. Electron. Conf., Busan, South Kores, Apr. 2019.